Synthesis, Structural Characterization, and Electrochemical Behavior of Copper(I) Complexes of Sterically Hindered Tris(3-*tert*-butyl- and 3,5-diphenylpyrazolyl)hydroborate Ligands

Susan M. Carrier, Christy E. Ruggiero, Robert P. Houser, and William B. Tolman*

University of Minnesota, 207 Pleasant Street S.E., Minneapolis, Minnesota 55455

Received June 11, 1993®

A series of Cu(I) complexes of sterically hindered tris(pyrazolyl)hydroborates $[Tp^{RR'}Cu]_2$ (R and R′ are the 3- and 5-pyrazolyl substituents, respectively; R = *t*-Bu, R′ = H or R = R′ = Ph) and $Tp^{RR'}CuL$ (R = *t*-Bu, R′ = H, L = CH_3CN; R = R′ = Ph, L = CH_3CN; R = R′ = Ph, L = 3,5-Ph_2pz = 3,5-diphenylpyrazole) were isolated and characterized by elemental analysis, variable-temperature ^1H NMR spectroscopy, osmometry, cyclic voltammetry, and, in the case of $[Tp^{t\text{-}Bu}Cu]_2$, $[Tp^{Ph2}Cu]_2$, and $Tp^{Ph2}Cu$(3,5-Ph_2pz), by X-ray crystallography. ($[Tp^{t\text{-}Bu}Cu]_2\cdot Et_2O$: $C_{46}H_{78}N_{12}B_2Cu_2O$, space group $P2_1/n$ (No. 14) at −101 °C with a = 19.001(8) Å, b = 13.629(8) Å, c = 21.490(7) Å, β = 113.01(3)°, V = 5122(8) Å^3, Z = 4, R = 0.082 and R_w = 0.075 for 3749 unique, observed reflections with $I > 2\sigma(I)$ and 541 variable parameters. $[Tp^{Ph2}Cu]_2\cdot 2CH_2Cl_2$: $C_{47}H_{38}N_6CuCl_4B$, space group $P2_1/n$ (No. 14) at −101 °C with a = 17.801(8) Å, b = 13.063(8) Å, c = 18.551(9) Å, β = 99.42(4)°, V = 4255(7) Å^3, Z = 4, R = 0.062 and R_w = 0.061 for 5552 unique, observed reflections with $I > 2\sigma(I)$ and 532 variable parameters. $Tp^{Ph2}Cu$(3,5-Ph_2pz)·CH_2Cl_2: $C_{61}H_{48}N_8BCuCl_2$, space group $P2_1/n$ (No. 14) at −101 °C with a = 10.308(7) Å, b = 29.105(9) Å, c = 17.158(8) Å, β = 93.54(5)°, V = 5138(8) Å^3, Z = 4, R = 0.069 and R_w = 0.061 for 5136 unique, observed reflections with $I > 2\sigma(I)$ and 658 variable parameters). Solution molecular weight data and ^1H NMR spectra of $[Tp^{t\text{-}Bu}Cu]_2$, which contains linear 2-coordinate Cu(I) ions bridged by η^2-$Tp^{t\text{-}Bu}$ ligands in the solid state, indicated that it retains its dimeric structure in solution, although the presence of a trace amount of a monomeric species could not be ruled out. A pyrazolyl ring exchange process occurs with $\Delta H^* = 11.7(5)$ kcal mol^{-1} and $\Delta S^* = -9(2)$ eu, as determined by line shape analysis of variable-temperature ^1H NMR spectra. $[Tp^{Ph2}Cu]_2$, in which η^3-Tp^{Ph2} ligands bridge between 3-coordinate Cu(I) ions in the solid state, apparently dissociates in solution to ill-defined species of lower molecular weight. ^1H NMR spectroscopy indicated that the pyrazole ligand in the monomeric, distorted tetrahedral $Tp^{Ph2}Cu$(3,5-Ph_2pz) is labile. Cyclic voltammograms of the $[Tp^{RR'}Cu]_2$ and $Tp^{RR'}Cu(CH_3CN)$ complexes in 0.1 M (TBA)PF_6/CH_2Cl_2 showed irreversible oxidations at high potentials (>+0.6 V vs SCE), but $Tp^{Ph2}Cu$(3,5-Ph_2pz) (same conditions) and $Tp^{t\text{-}Bu}Cu(CH_3CN)$ (in 10% CH_3CN/CH_2Cl_2 with 0.1 M (TBA)OTf) exhibited chemically reversible redox processes attributed to $Tp^{Ph2}Cu$(3,5-Ph_2pz)/$Tp^{Ph2}Cu$(3,5-Ph_2pz)$^+$ and $Tp^{t\text{-}Bu}Cu(CH_3CN)/Tp^{t\text{-}Bu}Cu(CH_3CN)^+$ couples with $E_{1/2}$ = +0.69 and +0.93 V vs SCE, respectively.

Introduction

An important strategy for the construction of transition metal complexes that model the structural, spectroscopic, and functional aspects of reactive metalloprotein active-site species is to use a multidentate supporting ligand that has large substituents oriented so that a bound metal ion will reside within a protected pocket of defined shape and size. Ideally, the steric fence provided by the pendant groups will inhibit destructive side reactions and control the nuclearity of the target compound(s), but will still allow desired metal-mediated biomimetic reactions to occur. Tris(pyrazolyl)hydroborates ($Tp^{RR'}$)[1–4] containing alkyl or aryl substituents at the pyrazoles' 3- and/or 5-positions[5–9] are exemplary ligands of this type that were recently found to be well-suited for bioinorganic model building. Particularly noteworthy examples include the use of $Tp^{t\text{-}Bu,Me}$ to prepare a mononuclear zinc hydroxide complex that resembles the catalytic unit of carbonic anhydrase,[10,11] Tp^{iPr2} to isolate iron[12,13] and manganese[14,15] complexes that model aspects of the active-site structure and reactivity of nonheme iron and manganese centers in proteins, Tp^{Me2} to bind molybdenum mimics of oxotransferases,[16,17] and Tp^{iPr2} and Tp^{Ph2} to synthesize spectroscopic analogs of type 1 cupric sites[18] and accurate structural and spectroscopic models for the dinuclear active center of oxyhemocyanin.[19–21]

In the latter work, Cu(I) complexes of the sterically hindered Tp ligands were reacted with O_2 to yield novel μ-(η^2:η^2)-peroxo

* Abstract published in *Advance ACS Abstracts,* October 1, 1993.

(1) The ligand nomenclature used has been described (Trofimenko, S. *Chem. rev.* **1993**, *93*, 943–980). The superscripts R and R′ refer to substituents attached to the 3- and 5-positions, respectively, of the pyrazolyl rings of the tris(pyrazolyl)hydroborate (Tp) ligand.
(2) Trofimenko, S. *Prog. Inorg. Chem.* **1986**, *34*, 115–210.
(3) Shaver, A. In *Comprehensive Coordination Chemistry*; Wilkinson, G., Gillard, R. D., McCleverty, J. A., Eds.; Pergamon Press: Oxford, U.K., 1987; Vol. 2, pp 245–259.
(4) Niedenzu, K.; Trofimenko, S. *Top. Curr. Chem.* **1986**, *131*, 1–37.
(5) Trofimenko, S.; Calabrese, J. C.; Thompson, J. S. *Inorg. Chem.* **1987**, *26*, 1507–1514.
(6) Trofimenko, S.; Calabrese, J. C.; Domaille, P. J.; Thompson, J. S. *Inorg. Chem.* **1989**, *28*, 1091–1101.
(7) Calabrese, J. C.; Domaille, P. J.; Thompson, J. S.; Trofimenko, S. *Inorg. Chem.* **1990**, *29*, 4429–4437.
(8) Calabrese, J. C.; Domaille, P. J.; Trofimenko, S.; Long, G. J. *Inorg. Chem.* **1991**, *30*, 2795–2801.
(9) Calabrese, J. C.; Trofimenko, S. *Inorg. Chem.* **1992**, *31*, 4810–4814.
(10) Alsfasser, R.; Trofimenko, S.; Looney, A.; Parkin, G.; Vahrenkamp, H. *Inorg. Chem.* **1991**, *30*, 4098–4100.
(11) Looney, A.; Parkin, G.; Alsfasser, R.; Ruf, M.; Vahrenkamp, H. *Angew. Chem., Int. Ed. Engl.* **1992**, *31*, 92–93.
(12) Kitajima, N.; Fukui, H.; Moro-oka, Y.; Mizutani, Y.; Kitagawa, T. *J. Am. Chem. Soc.* **1990**, *112*, 6402–6403.
(13) Kitajima, N.; Tamura, N.; Tanaka, M.; Moro-oka, Y. *Inorg. Chem.* **1992**, *31*, 3342–3343.
(14) Kitajima, N.; Singh, U. P.; Amagai, H.; Osawa, M.; Moro-oka, Y. *J. Am. Chem. Soc.* **1991**, *113*, 7757–7758.
(15) Kitajima, N.; Osawa, M.; Tanaka, M.; Moro-oka, Y. *J. Am. Chem. Soc.* **1991**, *113*, 8953–8955.
(16) Xiao, X.; Young, C. G.; Enemark, J. H.; Wedd, A. G. *J. Am. Chem. Soc.* **1992**, *114*, 9194–9195.
(17) Eagle, A. A.; Laughlin, L. J.; Young, C. G.; Tiekink, E. R. T. *J. Am. Chem. Soc.* **1992**, *114*, 9195–9197.
(18) Kitajima, N.; Fujisawa, K.; Tanaka, M.; Moro-oka, Y. *J. Am. Chem. Soc.* **1992**, *114*, 9232–9233.
(19) Kitajima, N.; Fujisawa, K.; Fujimoto, C.; Moro-oka, Y.; Hashimoto, S.; Kitagawa, T.; Toriumi, K.; Tatsumi, K.; Nakamura, A. *J. Am. Chem. Soc.* **1992**, *114*, 1277–1291.
(20) Baldwin, M. J.; Root, D. E.; Pate, J. E.; Fujisawa, K.; Kitajima, N.; Solomon, E. I. *J. Am. Chem. Soc.* **1992**, *114*, 10421–10431.
(21) Kitajima, N. *Adv. Inorg. Chem.* **1992**, *39*, 1–77.

0020-1669/93/1332-4889$04.00/0

dicopper(II) compounds.[19] Ill-defined oligomeric, $[Tp^{iPr2}Cu]_n$, and highly unusual monomeric, $[\eta^3\text{-}Tp^{R2}Cu]$ (R = Ph or *i*-Pr), structures were proposed for the Cu(I) compounds, but these formulations were based on analytical and ambient-temperature ^{1}H NMR spectroscopic data only. No conclusive data such as that which would be provided by an X-ray crystallographic analysis were reported for these useful Cu(I) starting materials. X-ray crystal structure and NMR solution studies of Cu(I) complexes of the less hindered ligands Tp^{R2} (R = H or Me) were performed over 15 years ago, which revealed that these compounds are dimeric in the solid state and highly fluxional in solution.[22] Interesting differences in the mode of ligand binding between $[TpCu]_2$, in which a pyrazolyl group symmetrically bridges 4-coordinate Cu(I) ions, and $[Tp^{Me2}Cu]_2$, in which the metals are essentially 3-coordinate, were observed. These differences were attributed to the divergent steric effects of the 3-substituents on the pyrazolyl rings, thus implying that new and unusual geometries might be attained in complexes of the more bulky $Tp^{RR'}$ ligands such as those used in the O_2 binding work.

We have begun to use related $Tp^{RR'}Cu^I$ starting materials to prepare novel mononuclear copper nitrosyl compounds as part of our research directed toward providing a chemical basis for the binding and subsequent interconversions of nitrogen oxides by copper proteins.[23-25] In order to fully understand the fundamentally important and biologically relevant reactions of the hindered $Tp^{RR'}Cu^I$ complexes with O_2 and NO, the lack of detailed information about their structural features needs to be addressed. In this paper we present the details of the syntheses of several new Cu(I) complexes ligated to Tp^{Ph2} and $Tp^{t\text{-}Bu}$ and the results of X-ray crystallographic, variable-temperature NMR spectroscopic, electrochemical, and solution molecular weight studies.[24] A detailed discussion of the use of some of the complexes discussed herein for the synthesis of copper nitrosyl adducts will be reported elsewhere.[25]

Experimental Section

General Procedures. All reagents, solvents, and gases used were obtained commercially and were of analytical grade. Dichloromethane and diethyl ether were distilled from CaH_2, and the former was stored over Linde Type 4A molecular sieves. Toluene and tetrahydrofuran were distilled from sodium benzophenone ketyl. Cuprous chloride was purchased from Mallinckrodt, purified by published procedures,[26] and stored under nitrogen. $[Cu(CH_3CN)_4]BF_4$,[27] $TlTp^{t\text{-}Bu}$,[5] and KTp^{Ph2} [19] were prepared according to literature methods. All complexes were synthesized and handled under an inert atmosphere using a Vacuum Atmospheres, Inc., glovebox or standard vacuum-line techniques. Infrared spectra were recorded as KBr pellets using a Perkin-Elmer 1600 series FTIR spectrophotometer. ^{1}H NMR spectra were obtained using either a Bruker 200-MHz, Bruker 300-MHz, or Varian 500-MHz NMR spectrometer, and peaks are reported in ppm downfield from an internal TMS reference. Elemental analyses were conducted by Atlantic Microlabs, Inc., of Norcross, GA. Solution molecular weight measurements were obtained by using an adaptation of the Signer method.[28]

$[Tp^{t\text{-}Bu}Cu]_2$. Cuprous chloride (0.162 g, 1.63 mmol) and $TlTp^{t\text{-}Bu}$ (0.935 g, 1.60 mmol) were stirred in THF (~20 mL) for 1 h. The solvent was removed under vacuum, and the remaining solid was extracted with hexanes (3 × 10 mL). Filtration of the extracts through a Celite pad followed by removal of solvent under vacuum yielded the product as a white powder in quantitative yield based on ligand (0.723 g, 0.80 mmol). X-ray-quality crystals of $[Tp^{t\text{-}Bu}Cu]_2{\cdot}Et_2O$ were obtained by slow evaporation of solvent from a solution of the complex in diethyl ether: ^{1}H NMR (500 MHz, toluene-d_8, T = 217 K) δ 1.06 (s, 18 H), 1.44 (s, 18 H), 1.49 (s, 18 H), 5.86 (d, J = 2.0 Hz, 2 H), 5.90 (d, J = 2.0 Hz, 2 H), 6.09 (d, J = 2.0 Hz, 2 H), 7.44 (d, J = 2.0 Hz, 4 H), 8.17 ppm (d, J = 2.0 Hz, 2 H); ^{13}C NMR (75 MHz, CD_2Cl_2 20 °C) δ 31.2 (br m), 32.7 (br m), 101.9 (br), 104.6 (m), 135.8 (br), 164.8 ppm (br); IR (KBr) 737, 773, 1073, 1163, 1203, 1360, 1507, 2375 [ν(BH)], 2962 cm^{-1}. Anal. Calcd for $C_{42}H_{68}N_{12}B_2Cu_2$: C, 56.69; H, 7.70; N, 18.89. Found: C, 56.82; H, 7.64; N, 18.60.

$[Tp^{Ph2}Cu]_2$. KTp^{Ph2} (1.18 g, 1.7 mmol) and cuprous chloride (0.170 g, 1.7 mmol) were stirred in THF (30 mL) for 30 min. The solvent was evaporated, the resulting solid was extracted with toluene (20 mL), and the extract was filtered through a Celite pad. Solvent was evaporated from the colorless filtrate to yield the product as a white solid (0.540 g, 43%). X-ray-quality crystals of $[Tp^{Ph2}Cu]_2{\cdot}2CH_2Cl_2$ were obtained directly from the reaction in 36% yield by extracting with CH_2Cl_2 instead of toluene, reducing the volume to <10 mL, and allowing the solution to stand at room temperature for 2–6 h. ^{1}H NMR (300 MHz, CD_2Cl_2) δ 6.33 (s, 3 H), 6.75–6.83 (m, 9 H), 6.91–6.93 (m, 6 H), 7.12–7.14 (m, 9 H), 7.43–7.46 ppm (m, 6H); ^{13}C NMR (75 MHz, CD_2Cl_2) δ 104.7, 126.3, 126.9, 127.1, 127.7, 129.4, 132.0, 132.1, 152.3, 154.2 ppm; IR (KBr) 567, 694, 766, 914, 1003, 1042, 1076, 1101, 1169, 1235, 1343, 1405, 1476, 1543, 1604, 2600 [ν(BH)], 3060 cm^{-1}. Anal. Calcd for $C_{90}H_{68}B_2Cu_2N_{12}$: C, 73.72; H, 4.67; N, 11.46. Found: C, 73.46; H, 4.66; N, 11.52.

$Tp^{t\text{-}Bu}Cu(CH_3CN)$. $TlTp^{t\text{-}Bu}$ (0.200 g, 0.475 mmol) and $[Cu(CH_3CN)_4]BF_4$ (0.150 g, 0.476 mmol) were stirred in CH_2Cl_2 (~10 mL) for 30 min. The mixture was filtered, and solvent was removed from the filtrate to afford a white powder. Recrystallization from toluene/hexanes yielded $Tp^{t\text{-}Bu}Cu(CH_3CN)$ as white needles (0.130 g, 56%): ^{1}H NMR (500 MHz, CD_2Cl_2) δ 1.43 (s, 27 H), 2.24 (s, 3 H), 5.99 (d, J = 1.1 Hz, 3 H), 7.47 ppm (d, J = 1.1 Hz, 3 H); ^{13}C NMR (125 MHz, CD_2Cl_2) δ 2.7, 30.6, 32.1, 100.5, 134.4, 161.7 ppm; IR (KBr) 735, 770, 1048, 1099, 1164, 1202, 1256, 1360, 1460, 1504, 2435 [ν(BH)], 2867, 2960 cm^{-1}. Anal. Calcd for $C_{23}H_{37}N_7BCu$: C, 57.25; H, 7.65; N, 20.40. Found: C, 56.86; H, 7.68; N, 20.18.

$Tp^{Ph2}Cu(CH_3CN)$. KTp^{Ph2} (0.913 g, 1.29 mmol) and $[Cu(CH_3CN)_4]BF_4$ (0.420 g, 1.33 mmol) were stirred in CH_2Cl_2 (30 mL) for 3 h. The solution was filtered through a Celite pad, and solvent was evaporated under vacuum to yield a slightly yellow solid. Recrystallization from CH_2Cl_2/Et_2O afforded fine white crystals of $Tp^{Ph2}Cu(CH_3CN)$ (0.547 g, 52%): ^{1}H NMR (500 MHz, CD_2Cl_2) δ 1.99 (s, 3 H), 6.55 (s, 3 H), 6.97–7.07 (m, 12 H), 7.25–7.28 (m, 3 H), 7.37–7.47 (m, 9 H), 7.99–8.00 ppm (d, J = 6.7 Hz, 6 H); ^{13}C NMR (125 MHz, CD_2Cl_2) δ 3.1, 104.6, 114.1, 127.8, 127.9, 128.0, 128.2, 128.3, 128.4, 129.4, 130.2, 132.8, 134.3, 150.2, 151.7 ppm; IR (KBr) 568, 670, 697, 766, 809, 915, 1005, 1029, 1072, 1117, 1171, 1235, 1341, 1460, 1479, 1542, 1604, 2268 [ν(CN)], 2621 [ν(BH)], 3043 cm^{-1}. Anal. Calcd for $C_{48.5}H_{40}BCl_2CuN_7$ [$Tp^{Ph2}Cu(CH_3CN){\cdot}0.5CH_2Cl_2$]: C, 69.88; H, 4.69; N, 12.00. Found: C, 69.82; H, 4.87; N, 11.98. The presence of the CH_2Cl_2 solvate was confirmed by ^{1}H NMR spectroscopy in $CDCl_3$.

$Tp^{Ph2}Cu(3,5\text{-}Ph_2pz)$. KTp^{Ph2} (0.727 g, 1.03 mmol), 3,5-diphenylpyrazole (0.225 g, 1.02 mmol), and cuprous chloride (0.103 g, 1.03 mmol) were stirred in THF (30 mL) for 30 min. The solvent was evaporated under reduced pressure, and the residue was extracted with CH_2Cl_2 (20 mL). The solution was filtered through a Celite pad, and solvent was removed from the light yellow filtrate under vacuum to give $Tp^{Ph2}Cu(3,5\text{-}Ph_2pz)$ as a faintly yellow solid (1.03 g, 90%). This solid was recrystallized from CH_2Cl_2/Et_2O to obtain X-ray-quality crystals. ^{1}H NMR (300 MHz, $CDCl_3$) δ 6.42 (s, 3 H), 6.54 (s, 1 H), 6.95–7.25 (m, 28 H), 7.46–7.48 (m, 6 H), 7.82–7.84 ppm (m, 6 H); ^{13}C NMR (75 MHz, CD_2Cl_2) δ 102.1, 104.7, 127.3, 127.5, 127.6, 127.7, 128.0, 129.7, 132.6, 133.7, 150.2, 151.9 ppm; IR (KBr) 564, 693, 758, 804, 855, 913, 1005, 1071, 1168, 1211, 1234, 1339, 1406, 1461, 1477, 1543, 1566, 2612 [ν(BH)], 3060, 3396 cm^{-1} [ν(NH)]. Anal. Calcd for $C_{61.5}H_{49}BCl_3CuN_8$ [$Tp^{Ph2}Cu(3,5\text{-}Ph_2pz){\cdot}0.5CH_2Cl_2$]: C, 68.34; H, 4.56; N, 10.37. Found: C, 67.76; H, 4.38; N, 10.65. The presence of CH_2Cl_2 solvate was corroborated by X-ray crystallography and ^{1}H NMR spectroscopy.

$[Tp^{Me2}Cu]_2$. This complex was prepared by a modification of the literature procedure that avoided the use of CO.[22] Cuprous chloride (0.153 g, 1.55 mmol) and KTp^{Me2} (0.478 g, 1.42 mmol) were stirred in THF (~30 mL) for 2–3 h. The solvent was evaporated under reduced pressure, and the remaining powder was extracted with benzene (50 mL). Filtration followed by removal of solvent from the filtrate under vacuum

(22) Mealli, C.; Arcus, C. S.; Wilkinson, J. L.; Marks, T. J.; Ibers, J. A. *J. Am. Chem. Soc.* **1976**, *98*, 711–718.
(23) Tolman, W. B. *Inorg. Chem.* **1991**, *30*, 4878–4880.
(24) Carrier, S. M.; Ruggiero, C. E.; Tolman, W. B.; Jameson, G. B. *J. Am. Chem. Soc.* **1992**, *114*, 4407–4408.
(25) Tolman, W. B.; Carrier, S. M.; Ruggiero, C. E.; Antholine, W. E.; Whittaker, J. W.; Cramer, C. J. *J. Am. Chem. Soc.*, in press.
(26) Perrin, D. D.; Armarego, W. L. F. *Purification of Laboratory Chemicals*; Pergamon Press: New York, 1988.
(27) Hathaway, B. J.; Holah, D. G.; Postlethwaite, J. D. *J. Chem. Soc.* **1961**, 3215–3218.
(28) Burger, B. J.; Bercaw, J. E. In *Experimental Organometallic Chemistry: A Practicum in Synthesis and Characterization*; Wayda, A. L., Darensbourg, M. Y., Eds.; ACS Symposium Series 357; American Chemical Society: Washington, DC, 1987; pp 79–98.

Table I. Crystallographic Data for $[Tp^{t\text{-}Bu}Cu]_2\cdot Et_2O$, $[Tp^{Ph2}Cu]_2\cdot 2CH_2Cl_2$, and $Tp^{Ph2}Cu(3,5\text{-}Ph_2pz)\cdot CH_2Cl_2$

	$[Tp^{t\text{-}Bu}Cu]_2\cdot Et_2O$	$[Tp^{Ph2}Cu]_2\cdot 2CH_2Cl_2$	$Tp^{Ph2}Cu(3,5\text{-}Ph_2pz)\cdot CH_2Cl_2$
formula	$C_{46}H_{78}N_{12}B_2Cu_2O$	$C_{47}H_{38}N_6CuCl_4B$	$C_{61}H_{48}N_8BCuCl_2$
fw	963.91	903.03	1038.86
space group	$P2_1/n$ (No. 14)	$P2_1/n$ (No. 14)	$P2_1/n$ (No. 14)
a (Å)	19.001(8)	17.801(8)	10.308(7)
b (Å)	13.629(8)	13.063(8)	29.105(9)
c (Å)	21.490(7)	18.551(9)	17.158(8)
β (deg)	113.01(3)	99.42(4)	93.54(5)
V (Å^3)	5122(8)	4255(7)	5138(8)
Z	4	4	4
ρ_{calcd} (g cm^{-3})	1.250	1.409	1.342
μ (cm^{-1})	8.76	8.07	5.77
T (°C)	−101	−101	−101
radiation, λ (Å)	Mo Kα, 0.710 69	Mo Kα, 0.710 69	Mo Kα, 0.710 69
$2\theta_{max}$ (deg)	48.2	52.0	50.1
tot. no. of data collected	8123	8863	9189
tot. no. of unique data	8123	8577	8646
tot. no. of unique data with $I > 2\sigma(I)$	3749	5552	5136
no. of variable params	541	532	658
R^a	0.082	0.062	0.069
$R_w{}^a$	0.075	0.061	0.061

^{a} $R = \sum||F_o| - |F_c||/\sum|F_o|$; $R_w = [(\sum w(|F_o| - |F_c|)^2/\sum wF_o^2)]^{1/2}$, where $w = 4F_o^2/s^2(F_o^2)$ and $s^2(F_o^2) = [S^2(C + R^2B + (pF_o^2)^2]/(Lp)^2$ with S = scan rate, C = total integrated peak count, R = ratio of scan time to background counting time, B = total background count, Lp = Lorentz–polarization factor, and p = p factor (0.05 for $[Tp^{t\text{-}Bu}Cu]_2\cdot Et_2O$ and 0.03 for $[Tp^{Ph2}Cu]_2\cdot 2CH_2Cl_2$ and $Tp^{Ph2}Cu(3,5\text{-}Ph_2pz)\cdot CH_2Cl_2$).

resulted in a white powder, which was recrystallized by cooling a CH_2Cl_2 (~25 mL) solution to −20° (0.295 g, 58%). ^{1}H NMR and FTIR data for the complex matched those reported previously.[22]

X-ray Crystallography. $[Tp^{t\text{-}Bu}Cu]_2\cdot Et_2O$. A colorless plate-shaped crystal of dimensions 0.55 × 0.35 × 0.10 mm was mounted on a glass fiber with heavy-weight oil and quickly placed under a cold N_2 stream on the diffractometer. All measurements were made on an Enraf-Nonius CAD-4 diffractometer with graphite-monochromated Mo Kα (λ = 0.710 69 Å) radiation. Important crystallographic information is summarized in Table I. Cell constants were obtained from a least squares refinement of the setting angles of 44 carefully centered reflections in the range $20.00 < 2\theta < 37.00°$. The intensity data were collected using the ω–2θ scan technique to a maximum 2θ value of 48.2°. An empirical absorption correction was applied, using the program DIFABS,[29] which resulted in transmission factors ranging from 0.80 to 1.09. The data were corrected for Lorentz and polarization effects, but no decay correction was needed.

The structure was solved by direct methods[30] using the TEXSAN[31] software package. Non-hydrogen atoms were refined either isotropically (solvent and B1) or anisotropically, and the H atoms were placed at calculated positions. Difference Fourier maps indicated the presence of a solvent molecule in the lattice (presumably an Et_2O molecule), but it was not ordered and a set of seven C atoms, C71–C77, was used to approximate it. The high R factors probably result from this crude modeling procedure. The maximum and minimum peaks on the final difference Fourier map corresponded to 0.81 and −0.64 e/Å^3, respectively. Neutral-atom scattering factors[32] and anomalous dispersion terms[33,34] were taken from the literature. ORTEP drawings of the structure appear in Figure 1. Selected bond lengths and angles are presented in Table II, and final atomic positional parameters and B(eq) values (excluding H atoms and atoms of solvent) are listed in Table III. Full tables of bond lengths and angles, atomic positional parameters, and final thermal parameters for non-hydrogen atoms are given in supplementary material Tables S1–S4.

$[Tp^{Ph2}Cu]_2\cdot 2CH_2Cl_2$. A colorless prism-shaped crystal of dimensions 0.45 × 0.45 × 0.35 mm was mounted on a glass fiber as described for $[Tp^{t\text{-}Bu}Cu]_2\cdot Et_2O$. Important crystallographic information is summarized in Table I. Cell constants were obtained from a least-squares refinement of the setting angles of 23 carefully centered reflections in the range $22.36 < 2\theta < 45.62°$, and the intensity data were collected as described for $[Tp^{t\text{-}Bu}Cu]_2\cdot Et_2O$ to a maximum 2θ value of 52.0°. An empirical absorption correction was applied using DIFABS, resulting in transmission factors ranging from 0.88 to 1.15, and no decay correction was needed.

The structure was solved by direct methods.[35,36] Non-hydrogen atoms were refined anisotropically, and the H atoms were placed at calculated positions. The maximum and minimum peaks in the final difference Fourier map corresponded to 1.01 and −0.68 e/Å^3, respectively. An ORTEP drawing of the structure is shown in Figure 2. Selected bond lengths and angles are presented in Table II, and final atomic positional parameters and B(eq) values (excluding H atoms, solvent atoms, and all phenyl atoms except the *ipso* carbons) are listed in Table IV. Full tables of bond lengths and angles, atomic positional parameters, and final thermal parameters for non-hydrogen atoms are given in supplementary material Tables S5–S8.

$Tp^{Ph2}Cu(3,5\text{-}Ph_2pz)\cdot CH_2Cl_2$. A colorless plate-shaped crystal of dimensions 0.60 × 0.50 × 0.20 mm was mounted on a glass fiber as described for $[Tp^{t\text{-}Bu}Cu]_2\cdot Et_2O$. Important crystallographic information is summarized in Table I. Cell constants were obtained from a least-squares refinement of the setting angles of 23 carefully centered reflections in the range $23.86 < 2\theta < 49.00°$, and the intensity data were collected as described for $[Tp^{t\text{-}Bu}Cu]_2\cdot Et_2O$ to a maximum 2θ value of 50.1°. No correction for decay was necessary. An empirical absorption correction was applied using DIFABS, resulting in transmission factors ranging from 0.80 to 1.33.

The structure was solved by direct methods.[35,36] Non-hydrogen atoms were refined anisotropically, and the H atoms were placed at calculated positions. The maximum and minimum peaks in the final difference Fourier map corresponded to 1.18 and −0.91 e/Å^3, respectively. An ORTEP drawing of the structure is shown in Figure 4. Selected bond lengths and angles are presented Table II, and final atomic positional parameters and B(eq) values (excluding H atoms, solvent atoms, and all phenyl atoms except the *ipso* carbons) are listed in Table V. Full tables of bond lengths and angles, atomic positional parameters, and final thermal parameters for non-hydrogen atoms are given in supplementary material Tables S9–S12.

Variable-Temperature NMR Spectroscopy and Simulations. Variable-temperature ^{1}H NMR spectra were obtained by using a Varian 500-MHz NMR spectrophotometer equipped with a Varian Unity 500 temperature regulator. Data were collected at temperatures ranging from 217 to 361 K for $[Tp^{t\text{-}Bu}Cu]_2$ and at 213 K and room temperature for $[Tp^{Ph2}Cu]_2$. The temperatures were calibrated over the low-temperature range using a methanol standard and above ambient temperatures using an ethylene glycol standard and are accurate to within ±1 K.[37] Line shape analyses of the *tert*-butyl peaks in the spectra of $[Tp^{t\text{-}Bu}Cu]_2$ were performed by using the dynamic NMR fitting program DNMR5[38] with a 3 × 3 exchange matrix predicted by the proposed intramolecular three site exchange as described in the text. Application of a correction for a slight linear dependence of the transverse relaxation time with temperature gave improved simulations. A plot of $\ln(k/T)$ vs $1/T$ was linear (R = 0.9996, Figure 6), thus allowing calculation of activation parameters according to the Eyring equation $\ln(k/T) = c' - \Delta H^*/RT + \Delta S^*/R$ (R = gas constant).

Electrochemistry. Electrochemical experiments were performed by using an EG&G Princeton Applied Research (PAR) VeraStat potentiostat driven by EG&G PAR Model 250 software. A three compartment,

(29) Walker, N.; Stuart, D. *Acta Crystallogr.* **1983**, *A39*, 158–166.
(30) Calabrese, J. C. PHASE: Patterson Heavy Atom Solution Extractor. Ph.D. Thesis, University of Wisconsin, Madison, WI, 1972.
(31) *TEXSAN-Texray Structure Analysis Package*; Molecular Structure Corp.: The Woodlands, TX, 1985.
(32) Cromer, D. T. *International Tables for X-ray Crystallography*; The Kynoch Press: Birmingham, U.K., 1974; Vol. IV, Table 2.2A.
(33) Ibers, J. A.; Hamilton, W. C. *Acta Crystallogr.* **1964**, *17*, 781.
(34) Cromer, D. T. *International Tables for X-ray Crystallography*; The Kynoch Press: Birmingham, U.K., 1974; Vol. IV, Table 2.3.1.
(35) Gilmore, C. J. *Appl. Crystallogr.* **1984**, *17*, 42–46.
(36) Beurskens, P. T.; DIRDIF: Technical Report 1984/1. Thesis, Crystallography Laboratory, Toernooiveld, 6525 Ed Nijmegen, The Netherlands, 1984.
(37) VanGeet, A. L. *Abstracts of Papers*; 10th Experimental NMR Conference; Mellon Institute: Pittsburgh, PA, 1969.
(38) DNMR5, modified for IBM-PC by C. B. LeMaster, C. L. LeMaster, and N. S. True; Quantum Chemistry Program Exchange No. QCMP059, Indiana University, Bloomington, IN.

Table II. Intramolecular Distances (Å) and Angles (deg) Relevant to the Copper Coordination Spheres in $[Tp^{t\text{-}Bu}Cu]_2 \cdot Et_2O$, $[Tp^{Ph2}Cu]_2 \cdot 2CH_2Cl_2$, and $Tp^{Ph2}Cu(3,5\text{-}Ph_2pz) \cdot CH_2Cl_2$

$[Tp^{t\text{-}Bu}Cu]_2$		$[Tp^{Ph2}Cu]_2$		$Tp^{Ph2}Cu(3,5\text{-}Ph_2pz)$	
Cu1···Cu2	3.284(8)	Cu1···Cu1′	2.544(2)	Cu1–N11	2.188(5)
Cu1–N11	1.874(9)	Cu1–N11	2.022(4)	Cu1–N21	2.205(5)
Cu1–N41	1.883(9)	Cu1–N21	2.010(4)	Cu1–N31	1.990(5)
Cu2–N31	1.882(9)	Cu1–N31	1.934(4)	Cu1–N41	1.960(5)
Cu2–N61	1.860(8)				
N11–Cu1–N41	176.7(4)	N11–Cu1–N21	100.0(2)	N11–Cu1–N21	90.3(2)
N31–Cu2–N61	176.5(4)	N11–Cu1–N31′	125.4(2)	N11–Cu1–N31	88.2(2)
		N21–Cu1–N31′	129.9(2)	N11–Cu1–N41	111.5(2)
				N21–Cu1–N31	93.5(2)
				N21–Cu1–N41	106.1(2)
				N31–Cu1–N41	151.7(2)

airtight, gas-adapted cell was used with a platinum disk working electrode and a platinum wire counter electrode separated from the working electrode by a sintered-glass frit. The reference electrode (SCE, Fisher Scientific liquid filled, cracked bead junction) was separated from the main compartment by a platinum wire/glass junction. Cyclic voltammograms were recorded under Ar on pure CH_2Cl_2 or 10(2)% CH_3CN/CH_2Cl_2 (v/v) solutions containing 0.1 M electrolyte [tetra-*n*-butylammonium hexafluorophosphate (TBAH), recrystallized from EtOAc/hexanes, or tetra-*n*-butylammonium trifluoromethanesulfonate ((TBA)OTf), recrystallized from CH_2Cl_2/Et_2O]. Potentials are reported vs SCE and are not corrected for the junction potential. The $E_{1/2}$ value for the Fc/Fc^+ couple was measured under the same conditions as those used for the compounds under study. In CH_2Cl_2/TBAH, $E_{1/2}$ = 0.453 V; in CH_2Cl_2/(TBA)OTf, $E_{1/2}$ = 0.473 V; in 10(2)% CH_3CN/CH_2Cl_2/TBAH, $E_{1/2}$ = 0.42(2) V; in 10(2)% CH_3CN/CH_2Cl_2/(TBA)OTf, $E_{1/2}$ = 0.44(2) V. No *iR* compensation was used.

Results

Syntheses. The nuclearity of the products of the reactions of $Tp^{t\text{-}Bu}$ and Tp^{Ph2} salts with Cu(I) starting materials depended on the presence or absence of additional species capable of coordinating to the metal ion. Treatment of CuCl with $TlTp^{t\text{-}Bu}$ or KTp^{Ph2} in THF resulted in the formation of the dimeric complexes $[Tp^{t\text{-}Bu}Cu]_2$ and $[Tp^{Ph2}Cu]_2$ in quantitative and 43% isolated yields, respectively (Scheme I). In the presence of CH_3CN or 3,5-diphenylpyrazole, however, reactions of $TlTp^{t\text{-}Bu}$ or KTp^{Ph2} with Cu(I) salts provided pseudotetrahedral monomers of general formula $Tp^{RR'}CuL$ (R = *t*-Bu, R′ = H, L = CH_3CN; R = R′ = Ph, L = CH_3CN; R = R′ = Ph, L = 3,5-diphenylpyrazole) in 50–90% isolated yields. An analogous monomer $Tp^{Ph2}Cu(Me_2CO)$ was also reported to form when similar preparative chemistry was carried out in acetone.[19,39] All of the compounds were isolated as colorless to very pale yellow solids, and their formulations were supported by ^1H NMR spectroscopy, by elemental analysis, and, in the cases of $[Tp^{t\text{-}Bu}Cu]_2$, $[Tp^{Ph2}Cu]_2$, and $Tp^{Ph2}Cu(3,5\text{-}Ph_2pz)$, by X-ray crystallography. ^{13}C NMR spectra for the compounds were recorded but were generally uninformative due to overlapping and/or broadness of the observed peaks.

Solid-State Structures. $[Tp^{t\text{-}Bu}Cu]_2 \cdot Et_2O$. Two ORTEP representations of the X-ray crystal structure of this dimer are shown in Figure 1, one showing the full structure (left) and the other showing the core of the molecule with *tert*-butyl groups removed for clarity (right). Important bond lengths and angles are listed in Table II, and selected positional parameters are provided in Table III. The discrepancy indices and the estimated standard deviations in bond lengths and angles for the structure are not optimum, primarily because of the presence of highly disordered solvent molecules in the crystal which were modeled rather crudely. Higher quality structures of this and an analogous $Tp^{t\text{-}Bu,Me}$ compound which generally agree with ours have been determined.[40]

Each $Tp^{t\text{-}Bu}$ ligand in the molecule bridges between the copper(I) ions by binding via one pyrazolyl group to each metal ion. The third pyrazolyl ring in each ligand is not coordinated to a copper center and is turned so that its potential N-donor atom (N21 or N51) is directed away from the dicopper(I) core. The steric influences of the 3-*tert*-butyl groups presumably are responsible for adoption of this unusual binding mode of the $Tp^{t\text{-}Bu}$ ligands. Both free pyrazolyl rings in the dimer are disposed on the same side of the molecule (directed out of the page in the drawings in Figure 1), thus causing all of the pyrazolyl rings to reside in chemically inequivalent environments. This asymmetry has important consequences for solution NMR spectroscopic studies (*vide infra*).

The Cu(I) ions are 2-coordinate with close to linear geometries (average N–Cu–N angle = 176.6°), and the N–Cu–N vectors are twisted relative to one another (dihedral angle = 72.4°). The relatively long distance of 3.284(8) Å between the metal ions suggests that there is little, if any, interaction between them. The 3-*tert*-butyl substituents on the ligands appear to prevent approach of any additional ligands in the crystal by providing a steric "fence" surrounding the dimetal core of the complex. As is typical for copper(I) complexes with such a low coordination number,[41–44] the Cu–N distances are short (1.86–1.88 Å). Metal–ligand distances in 3- and 4-coordinate copper(I) complexes of aromatic N-donors are usually longer (>1.9 Å),[45] an observation confirmed by the X-ray crystal structures of $[Tp^{Ph2}Cu]_2$ and $Tp^{Ph2}Cu(3,5\text{-}Ph_2pz)$ reported herein.

$[Tp^{Ph2}Cu]_2 \cdot 2CH_2Cl_2$. An ORTEP representation of this dimer is shown in Figure 2 with only the *ipso* carbon atoms of the phenyl groups drawn for clarity. A full view of the molecule is provided in the supplementary material. Important bond lengths and angles are listed in Table II, and selected positional parameters are given in Table IV.

The overall dimeric structure of $[Tp^{Ph2}Cu]_2$ closely resembles that of $[Tp^{Me2}Cu]_2$ that was reported previously,[22] although significant differences exist between the core geometries of the two structures. This is apparent from the identical views of the two molecules perpendicular to their Cu···Cu vectors shown in Figure 3. Both compounds have a crystallographically imposed center of symmetry with each Tp ligand binding via two pyrazolyl groups to one copper(I) ion and via the third pyrazolyl donor to the other metal center. A similar bridging arrangement of tris(imidazolyl)methoxymethane and tris(4,5-dihydrooxazolyl)methylamine ligands analogous to Tp has been observed previous-

(39) Kitajima, N.; Fujisawa, K.; Fujimoto, C.; Moro-oka, Y. *Chem. Lett.* **1989**, 421–424.
(40) Parkin, G. Personal communication.
(41) Sorrell, T. N.; Jameson, D. L. *J. Am. Chem. Soc.* **1983**, *105*, 6013–6018.
(42) Hendriks, H. M. J.; Birker, P. J. M. W. L.; Rijn, J. v.; Verschoor, G. C.; Reedijk, J. *J. Am. Chem. Soc.* **1982**, *104*, 3607–3617.
(43) Power, P. P.; Ruhlandt-Senge, K.; Shoner, S. C. *Inorg. Chem.* **1991**, *30*, 5013–5015.
(44) Evans, D. A.; Woerpel, K. A.; Scott, M. J. *Angew. Chem., Int. Ed. Engl.* **1992**, *31*, 430–432.
(45) Karlin, K. D.; Hayes, J. C.; Gultneh, Y.; Cruse, R. W.; McKown, J. W.; Hutchinson, J. P.; Zubieta, J. *J. Am. Chem. Soc.* **1984**, *106*, 2121–2128 and references therein.

Table III. Selected Positional Parameters for $[Tp^{t\text{-}Bu}Cu]_2\cdot Et_2O$

atom	x	y	z	B(eq) (Å²)
Cu1	0.12995(8)	0.4509(1)	0.41865(7)	1.62(6)
Cu2	0.29128(8)	0.5730(1)	0.46348(7)	1.63(6)
N11	0.0503(5)	0.5296(6)	0.3609(4)	1.1(4)
N12	0.0587(5)	0.6309(6)	0.3600(4)	1.4(4)
N21	0.0958(5)	0.8535(7)	0.3952(5)	1.8(4)
N22	0.1360(5)	0.7846(6)	0.3743(5)	1.7(4)
N31	0.2397(5)	0.6353(7)	0.5116(5)	1.7(4)
N32	0.1670(5)	0.6688(7)	0.4742(5)	1.6(4)
N41	0.2058(5)	0.3668(6)	0.4768(5)	1.4(4)
N42	0.2650(5)	0.3439(7)	0.4582(5)	1.7(4)
N51	0.3250(5)	0.2084(7)	0.3752(5)	1.9(4)
N52	0.2620(5)	0.2686(7)	0.3493(5)	1.8(4)
N61	0.3444(5)	0.5191(6)	0.4151(4)	1.2(4)
N62	0.3274(5)	0.4294(7)	0.3845(4)	1.4(4)
C13	−0.0055(7)	0.6689(8)	0.3147(6)	1.8(5)
C14	−0.0564(7)	0.5958(9)	0.2863(6)	1.9(5)
C15	−0.0205(6)	0.5081(8)	0.3155(5)	1.2(5)
C16	−0.0485(7)	0.4032(8)	0.2988(6)	2.0(5)
C17	−0.0299(7)	0.3463(9)	0.3654(7)	2.9(6)
C18	−0.0086(8)	0.355(1)	0.2584(7)	3.6(7)
C19	−0.1345(8)	0.403(1)	0.2606(7)	3.8(7)
C23	0.1671(7)	0.8250(9)	0.3346(9)	2.3(6)
C24	0.1494(7)	0.923(1)	0.3280(6)	2.6(6)
C25	0.1047(7)	0.9363(8)	0.3663(6)	2.1(5)
C26	0.0675(7)	1.0306(8)	0.3746(6)	2.2(5)
C27	0.0293(8)	1.020(1)	0.4239(7)	3.9(7)
C28	0.0116(8)	1.064(1)	0.3063(7)	4.3(7)
C29	0.1293(9)	1.111(1)	0.4006(7)	4.1(7)
C33	0.1362(7)	0.7032(9)	0.5157(6)	1.9(5)
C34	0.1906(7)	0.6945(8)	0.5815(6)	1.9(5)
C35	0.2539(7)	0.6514(8)	0.5761(6)	1.6(5)
C36	0.3298(6)	0.6284(8)	0.6319(6)	1.5(5)
C37	0.3601(7)	0.527(1)	0.6233(6)	3.4(6)
C38	0.3894(7)	0.705(1)	0.6325(7)	3.6(6)
C39	0.3234(8)	0.633(1)	0.7006(6)	3.5(6)
C43	0.3150(7)	0.2871(9)	0.5063(6)	2.1(5)
C44	0.2889(8)	0.2730(9)	0.5565(6)	2.6(6)
C45	0.2219(6)	0.3244(8)	0.5372(6)	1.5(5)
C46	0.1672(7)	0.3309(9)	0.5726(6)	2.1(5)
C47	0.2122(8)	0.312(1)	0.6590(7)	4.4(7)
C48	0.1061(8)	0.249(1)	0.5485(7)	3.4(7)
C49	0.1262(8)	0.431(1)	0.5632(6)	3.4(6)
C53	0.2159(7)	0.2361(9)	0.2879(6)	1.9(5)
C54	0.2463(7)	0.1552(8)	0.2729(6)	2.3(5)
C55	0.3149(7)	0.1400(8)	0.3282(6)	1.8(5)
C56	0.3777(7)	0.0647(8)	0.3388(6)	2.1(5)
C57	0.432(1)	0.105(1)	0.309(1)	6.0(9)
C58	0.3446(8)	−0.031(1)	0.3053(8)	5.5(8)
C59	0.423(1)	0.046(1)	0.4145(7)	5.9(8)
C63	0.3696(7)	0.4143(8)	0.3476(6)	1.8(5)
C64	0.4150(7)	0.496(1)	0.3534(6)	2.0(5)
C65	0.3973(6)	0.5590(8)	0.3970(5)	1.0(2)
C66	0.4345(6)	0.6585(8)	0.4223(6)	1.9(5)
C67	0.3748(7)	0.7357(8)	0.4173(6)	2.3(5)
C68	0.4791(7)	0.6912(9)	0.3810(6)	2.8(6)
C69	0.4896(8)	0.6454(8)	0.4964(6)	2.8(5)
B1	0.1387(8)	0.677(1)	0.3957(7)	1.5(3)
B2	0.2599(7)	0.365(1)	0.3846(6)	1.2(5)

ly in dicopper(I) complexes.[46,47] The 3-phenyl or -methyl substituents in $[Tp^{Ph2}Cu]_2$ and $[Tp^{Me2}Cu]_2$, respectively, are smaller than the 3-*tert*-butyl groups in $[Tp^{t\text{-}Bu}Cu]_2$, thus allowing the copper(I) ions to become 3-coordinate in the former structures. As expected for the increased coordination number, the Cu–N bond distances are substantially longer than those in $[Tp^{t\text{-}Bu}Cu]_2$; average Cu–N distances are 1.99 Å for $[Tp^{Ph2}Cu]_2$ and 1.97 Å for $[Tp^{Me2}Cu]_2$. In addition, similar coordination geometries for the copper(I) centers are evident in $[Tp^{Ph2}Cu]_2$ and $[Tp^{Me2}Cu]_2$, both of which can be best described as having distorted trigonal planar metal ions. The N–Cu–N angles ranging from 98 to 140° (Table II) comprise the main distortion from the ideal trigonal shape, although in each molecule the sum of these angles is close

(46) Sorrell, T. N.; Borovik, A. S. *J. Am. Chem. Soc.* **1987**, *109*, 4255–4260.
(47) Sorrell, T. N.; Pigge, F. C.; White, P. S. *Inorg. Chim. Acta*, in press.

Table IV. Selected Positional Parameters for $[Tp^{Ph2}Cu]_2\cdot 2CH_2Cl_2$

atom	x	y	z	B(eq) (Å²)
Cu1	0.00268(3)	0.07525(5)	0.04387(3)	1.35(2)
N11	−0.0967(2)	0.1192(3)	−0.0173(2)	1.3(1)
N12	−0.1638(2)	0.0684(3)	−0.0124(2)	1.2(1)
N21	−0.369(2)	0.0022(3)	0.1254(2)	1.3(2)
N22	−0.1160(2)	0.0018(3)	0.1157(2)	1.2(2)
N31	−0.1007(2)	−0.1383(3)	−0.0423(2)	1.2(1)
N32	−0.1512(2)	−0.1266(3)	0.0055(2)	1.2(1)
C13	−0.2232(3)	0.1211(4)	−0.0490(3)	1.4(2)
C14	−0.1956(3)	0.2076(4)	−0.0781(3)	1.7(2)
C15	−0.1172(3)	0.2042(4)	−0.0580(3)	1.5(2)
C23	−0.1388(3)	0.0176(4)	0.1811(3)	1.6(2)
C24	−0.0757(3)	0.0231(4)	0.2338(3)	1.7(2)
C25	−0.0131(3)	0.0152(4)	0.1972(3)	1.5(2)
C33	−0.2010(3)	−0.2070(4)	−0.0021(3)	1.5(2)
C34	−0.1838(3)	−0.2702(4)	−0.0566(3)	1.7(2)
C35	−0.1211(3)	−0.2256(4)	−0.0802(3)	1.5(2)
C101	−0.3042(3)	0.0911(4)	−0.0543(2)	1.6(2)
C102	−0.3561(3)	0.1659(4)	−0.0420(3)	2.4(2)
C103	−0.4334(3)	0.1430(5)	−0.0494(3)	3.2(3)
C104	−0.4591(3)	0.0465(5)	−0.0694(3)	3.1(3)
C105	−0.4085(3)	−0.0276(5)	−0.0813(3)	2.9(2)
C106	−0.3310(3)	−0.0069(4)	−0.0743(3)	2.1(2)
C111	−0.0622(3)	0.2829(4)	−0.0736(3)	1.6(2)
C112	0.0089(3)	0.2579(4)	−0.0909(3)	1.9(2)
C113	0.0568(3)	0.3360(4)	−0.1067(3)	2.4(2)
C114	0.0351(3)	0.4371(4)	−0.1059(3)	2.9(2)
C115	−0.0360(3)	0.4619(4)	−0.0893(3)	3.1(3)
C116	−0.0842(3)	0.3852(4)	−0.0734(3)	2.4(2)
C201	−0.2191(3)	0.0352(4)	0.1903(3)	1.8(2)
C202	−0.2647(3)	0.1072(4)	0.1487(3)	2.7(2)
C203	−0.3373(3)	0.1273(5)	0.1619(3)	3.5(3)
C204	−0.3653(3)	0.0776(6)	0.2168(3)	3.9(3)
C205	−0.3204(3)	0.0070(5)	0.2694(3)	3.3(3)
C206	−0.2475(3)	−0.0148(4)	0.2472(3)	2.5(2)
C211	0.0675(3)	0.0224(4)	0.2303(3)	1.6(2)
C212	0.0886(3)	0.0611(4)	0.3015(3)	2.4(2)
C213	0.1635(3)	0.0667(5)	0.3333(3)	3.0(2)
C214	0.2204(3)	0.0353(5)	0.2966(3)	3.0(3)
C215	0.2014(3)	−0.0022(5)	0.2263(5)	2.6(2)
C216	0.1262(3)	−0.0093(4)	0.1936(3)	2.1(2)
C301	−0.2617(3)	−0.2257(4)	0.0420(3)	1.8(2)
C302	−0.2495(3)	−0.2160(4)	0.1179(3)	2.3(2)
C303	−0.3066(4)	−0.2418(4)	0.1574(3)	3.1(3)
C304	−0.3757(4)	−0.2776(5)	0.1216(4)	3.7(3)
C305	−0.3886(3)	−0.2878(4)	0.0464(4)	3.3(3)
C306	−0.3326(3)	−0.2610(4)	0.0070(3)	2.4(2)
C311	−0.0800(3)	−0.2638(3)	−0.1382(3)	1.5(2)
C312	−0.0002(3)	−0.2633(4)	−0.1294(3)	1.9(2)
C313	0.0351(3)	−0.2995(4)	−0.1850(3)	2.3(2)
C314	−0.0065(3)	−0.3398(4)	−0.2478(3)	2.8(2)
C315	−0.0848(3)	−0.3431(5)	−0.2562(3)	2.9(3)
C316	−0.1214(3)	−0.3050(4)	−0.2016(3)	2.2(2)
B1	−0.1664(3)	−0.0218(4)	0.0420(3)	1.3(2)

to 360° (355°). Thus, only minor deviations from planarity are found for the copper coordination spheres in both structures (the copper ions reside 0.243 and 0.245 Å above the plane of N-donor atoms in $[Tp^{Ph2}Cu]_2$ and $[Tp^{Me2}Cu]_2$, respectively).

It is evident from the drawings in Figure 3, however, that the increased steric influences of the 3,5-phenyl substituents relative to the 3,5-methyl groups cause the core of $[Tp^{Ph2}Cu]_2$ to be substantially distorted compared to $[Tp^{Me2}Cu]_2$. The Cu···Cu distance is longer in $[Tp^{Ph2}Cu]_2$ [2.544(2) Å vs 2.507(1) Å]. More significantly, a short distance between Cu and N5′ of 2.777(4) Å in $[Tp^{Me2}Cu]_2$ suggests that there is some bridging interactions in this molecule; i.e., a "semibridging" pyrazolyl group is present.[22] In $[Tp^{Ph2}Cu]_2$, however, the analogous distance Cu1–N21′ is 3.125 Å, which is definitely nonbonding (Figure 3). Thus, the pyrazolyl ring containing N21′, N22′, C23′, C24′, and C25′ in $[Tp^{Ph2}Cu]_2$ is shifted away from the dicopper(I) core to a nonbridging position. We hypothesize that this distortion and the increased Cu···Cu distance in $[Tp^{Ph2}Cu]_2$ result from nonbonding interactions among the bulky phenyl substituents that

Table V. Selected Positional Parameters for $Tp^{Ph2}Cu(3,5\text{-}Ph_2pz)\cdot CH_2Cl_2$

atom	x	y	z	B(eq) (Å²)
Cu1	0.18407(8)	0.24597(2)	0.14870(4)	2.21(3)
N11	0.3246(5)	0.3024(2)	0.1556(3)	1.8(2)
N12	0.2635(5)	0.3434(1)	0.1624(3)	1.7(2)
N21	0.1004(5)	0.2704(2)	0.2564(3)	2.0(2)
N22	0.1015(5)	0.3172(1)	0.2593(3)	1.8(2)
N31	0.0684(5)	0.2854(2)	0.0799(3)	1.9(2)
N32	0.0314(5)	0.3255(1)	0.1163(3)	1.9(2)
N41	0.2674(5)	0.1870(2)	0.1750(3)	2.0(2)
N42	0.3646(5)	0.1898(2)	0.2331(3)	2.2(2)
C13	0.3488(6)	0.3789(2)	0.1551(3)	2.2(3)
C14	0.4680(6)	0.3593(2)	0.1447(3)	1.9(3)
C15	0.4509(6)	0.3117(2)	0.1438(3)	2.0(3)
C23	0.0683(6)	0.3319(2)	0.3313(3)	1.9(3)
C24	0.0462(6)	0.2933(2)	0.3748(3)	2.4(3)
C25	0.0674(6)	0.2556(2)	0.3270(3)	2.0(2)
C33	−0.0652(6)	0.3460(2)	0.0721(3)	2.1(3)
C34	−0.0909(6)	0.3199(2)	0.0071(3)	2.0(3)
C35	−0.0063(6)	0.2824(2)	0.0137(3)	2.0(3)
C43	0.4203(6)	0.1486(2)	0.2488(3)	2.2(3)
C44	0.3577(6)	0.1178(2)	0.2000(4)	2.3(3)
C45	0.2637(6)	0.1423(2)	0.1548(3)	2.2(3)
C101	0.3135(6)	0.4276(2)	0.1585(3)	2.2(3)
C102	0.2012(7)	0.4451(2)	0.1191(4)	2.6(3)
C103	0.1724(8)	0.4911(2)	0.1229(4)	3.6(4)
C104	0.2532(8)	0.5208(2)	0.1658(4)	3.7(4)
C105	0.3644(8)	0.5041(2)	0.2038(4)	3.6(4)
C106	0.3948(7)	0.4579(2)	0.1997(4)	3.1(3)
C111	0.5469(6)	0.2759(2)	0.1348(3)	2.2(3)
C112	0.6749(7)	0.2826(2)	0.1630(4)	2.7(3)
C113	0.7676(6)	0.2485(3)	0.1549(4)	3.6(3)
C114	0.7340(8)	0.2077(2)	0.1208(4)	3.4(4)
C115	0.6074(8)	0.2001(2)	0.0909(4)	3.2(3)
C116	0.5144(7)	0.2345(2)	0.0987(3)	2.5(3)
C201	0.0668(7)	0.3809(2)	0.3541(3)	2.3(3)
C202	0.1679(6)	0.4105(2)	0.3396(4)	2.6(3)
C203	0.1626(7)	0.4562(2)	0.3600(4)	3.3(3)
C204	0.0548(8)	0.4732(2)	0.3945(4)	4.1(4)
C205	−0.0448(8)	0.4443(2)	0.4101(5)	4.1(4)
C206	−0.0406(7)	0.3983(2)	0.3907(4)	3.4(3)
C211	0.0577(6)	0.2065(2)	0.3449(3)	2.1(3)
C212	0.0764(6)	0.1915(2)	0.4221(4)	2.5(3)
C213	0.0680(7)	0.1455(2)	0.4403(4)	2.9(3)
C214	0.0428(7)	0.1134(2)	0.3823(4)	3.3(3)
C215	0.0252(7)	0.1279(2)	0.3049(4)	3.0(3)
C216	0.0301(6)	0.1741(2)	0.2872(3)	2.3(3)
C301	−0.1309(6)	0.3888(2)	0.0953(3)	2.0(3)
C302	−0.1570(6)	0.3973(2)	0.1737(4)	2.5(3)
C303	−0.2213(7)	0.4368(2)	0.1936(4)	3.3(3)
C304	−0.2654(7)	0.4674(2)	0.1359(4)	3.6(4)
C305	−0.2424(8)	0.4589(2)	0.0587(4)	3.7(4)
C306	−0.1764(7)	0.4199(2)	0.0393(4)	2.9(3)
C311	0.0115(6)	0.2452(2)	−0.0422(3)	2.0(2)
C312	−0.0911(6)	0.2312(2)	−0.0922(3)	2.6(3)
C313	−0.0752(8)	0.1981(2)	−0.1488(4)	3.2(3)
C314	0.0460(8)	0.1793(2)	−0.1568(4)	3.5(4)
C315	0.1489(7)	0.1930(2)	−0.1073(4)	3.4(3)
C316	0.1319(7)	0.2258(2)	−0.0512(4)	2.7(3)
C401	0.5275(6)	0.1424(2)	0.3085(4)	2.4(3)
C402	0.5396(7)	0.1001(2)	0.3466(4)	3.4(3)
C403	0.6362(8)	0.0932(3)	0.4047(4)	4.2(4)
C404	0.7229(7)	0.1278(3)	0.4254(4)	3.9(4)
C405	0.7133(7)	0.1693(3)	0.3860(4)	3.5(4)
C406	0.6169(7)	0.1768(2)	0.3277(4)	3.0(3)
C411	0.1693(7)	0.1233(2)	0.0959(4)	2.4(3)
C412	0.1944(8)	0.0802(2)	0.0639(4)	4.2(4)
C413	0.108(1)	0.0602(3)	0.0105(5)	5.2(5)
C414	−0.0067(8)	0.0824(3)	−0.0125(4)	4.2(4)
C415	−0.0326(7)	0.1245(2)	0.0182(4)	3.2(3)
C416	0.0545(7)	0.1448(2)	0.0719(4)	2.5(3)
B1	0.1209(7)	0.3449(2)	0.1843(4)	1.8(3)

are accentuated relative to the analogous forces present in its 3,5-dimethyl-substituted congener.

$Tp^{Ph2}Cu(3,5\text{-}Ph_2pz)\cdot CH_2Cl_2$. Figure 4 shows an ORTEP representation of this monomeric complex. Important bond lengths and angles are listed in Table II, and selected positional parameters are given in Table V.

Scheme I

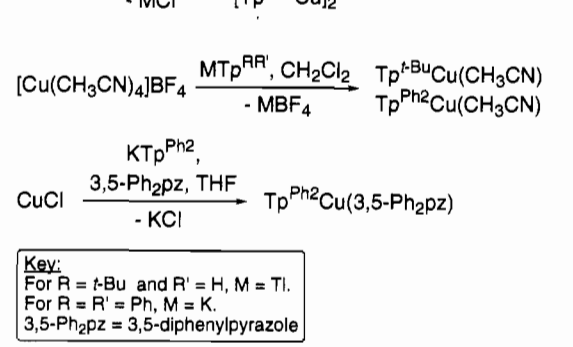

Tridentate coordination of the Tp^{Ph2} ligand and monodentate binding of 3,5-diphenylpyrazole to a single copper(I) ion are evident in the X-ray crystal structure of $Tp^{Ph2}Cu(3,5\text{-}Ph_2pz)$. Continuing the trend mentioned above, Cu–N bond distances in this tetravalent complex are lengthened, on average, compared to those of the compounds with lower coordination numbers (average Cu–N = 2.09 Å). Similar bond distances have been recorded for other 4-coordinate Cu(I) compounds with aromatic N-donors,[45,48–59] including pseudotetrahedral $Tp^{RR'}Cu^{I}L$ complexes.[19,59] A particularly noteworthy aspect of the structure of $Tp^{Ph2}Cu(3,5\text{-}Ph_2pz)$ is the high degree of distortion away from local (CuN_4) C_{3v} symmetry evidenced by the N31–Cu–N41 angle of 151.7(2)°. Steric interactions between the phenyl groups on the Tp^{Ph2} and 3,5-diphenylpyrazole ligands appear to be responsible for the observed displacement of the latter away from the position normally occupied in analogous $\sim C_{3v}$-symmetric tetradentate copper(I) monomers.[19,59]

Solution Structures. The ^1H NMR spectrum of $[Tp^{t\text{-}Bu}Cu]_2$ at room temperature contained broad peaks which sharpened upon cooling to three sets of 3-*tert*-butylpyrazole hydrogen resonances in a 1:1:1 ratio. As shown by the spectra in Figure 5, the three *tert*-butyl peaks apparent in the low-temperature-limiting spectrum (217 K) coalesce as the sample is warmed (361 K) to yield a single resonance. The presence of three inequivalent sets of pyrazole signals at low temperature is consistent with adoption of an asymmetric dimeric structure for the complex in solution similar to that which was observed in the solid state by X-ray crystallography. Further support for retention of the dimeric geometry of the complex in solution was obtained by osmometric molecular weight measurements [calculated MW =

(48) Lewin, A. H.; Michl, R. J.; Ganis, P.; Lepore, U.; Avitabile, G. *J. Chem. Soc., Chem. Commun.* **1971**, 1400–1401.
(49) Clegg, W.; Acott, S. R.; Garner, C. D. *Acta Crystallogr.* **1984**, *C40*, 768–769.
(50) Burke, P. J.; McMillin, D. R.; Robinson, W. R. *Inorg. Chem.* **1980**, *19*, 1211–1214.
(51) Hoffmann, S. K.; Corvan, P. J.; Singh, P.; Sethulekshmi, C. N.; Metzger, R. M.; Hatfield, W. E. *J. Am. Chem. Soc.* **1983**, *105*, 4608–4617.
(52) Hämäläinen, R.; Ahlgren, M.; Terpeinen, U.; Raikas, T. *Cryst. Struct. Commun.* **1979**, *8*, 74–80.
(53) Healy, P. C.; Engelhardt, L. M.; Patrick, V. A.; White, A. H. *J. Chem. Soc., Dalton Trans.* **1985**, 2541–2545.
(54) Karlin, K. D. *Inorg. Chim. Acta* **1982**, *64*, L219–L220.
(55) Karlin, K. D.; Cruse, R. W.; Gultneh, Y.; Farooq, A.; Hayes, J. C.; Zubieta, J. *J. Am. Chem. Soc.* **1987**, *109*, 2668–2679.
(56) Karlin, K. D.; Haka, M. S.; Cruse, R. W.; Meyer, G. J.; Farooq, A.; Gulneh, Y.; Hayes, J. C.; Zubieta, J. *J. Am. Chem. Soc.* **1988**, *110*, 1196–1207.
(57) Karlin, K. D.; Ghosh, P.; Cruse, R. W.; Farooq, A.; Gultneh, Y.; Jacobson, R. R.; Blackburn, N. J.; Strange, R. W.; Zubieta, J. *J. Am. Chem. Soc.* **1988**, *110*, 6769–6780.
(58) Tyeklár, Z.; Jacobson, R. R.; Wei, N.; Murthy, N. N.; Zubieta, J.; Karlin, K. D. *J. Am. Chem. Soc.* **1993**, *115*, 2677–2689.
(59) Churchill, M. R.; DeBoer, B. G.; Rotella, F. J.; Salah, O. M. A.; Bruce, M. I. *Inorg. Chem.* **1975**, *14*, 2051–2056.

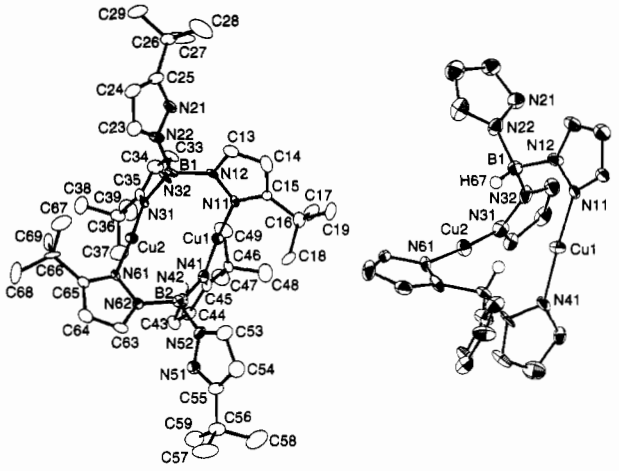

Figure 1. ORTEP drawings of $[Tp^{t\text{-}Bu}Cu]_2 \cdot Et_2O$ showing 60% probability thermal ellipsoids for all non-hydrogen atoms (excluding disordered Et_2O solvate molecule): left, view of entire molecule (excluding hydrogen atoms); right, core of molecule with *tert*-butyl groups omitted for clarity (labels provided only for selected non-carbon atoms).

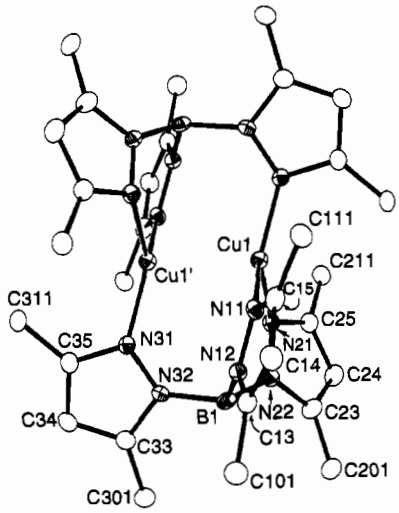

Figure 2. ORTEP drawing of $[Tp^{Ph2}Cu]_2 \cdot 2CH_2Cl_2$ showing 50% probability thermal ellipsoids for all non-hydrogen atoms (excluding CH_2Cl_2 solvate molecules). Only the *ipso* carbons of the phenyl rings are shown for clarity (see supplementary material for drawing that includes all non-hydrogen atoms of the phenyl rings).

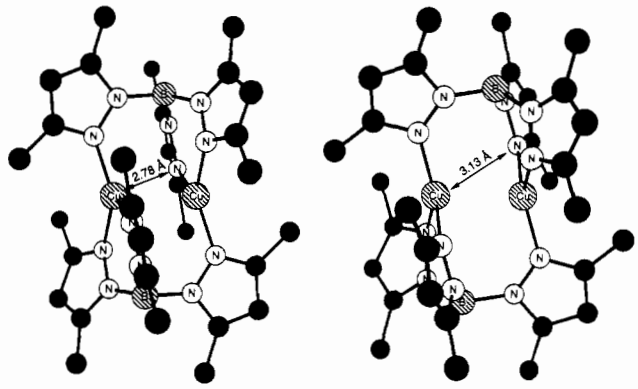

Figure 3. Drawings of $[Tp^{Me2}Cu]_2$ (left; from the published coordinates[22]) and $[Tp^{Ph2}Cu]_2$ (right; only *ipso* carbons of phenyl rings shown) viewed perpendicular to the Cu···Cu axis.

890, found MW = 950(80)]. Possible mechanisms which could account for the variable-temperature NMR behavior of $[Tp^{t\text{-}Bu}Cu]_2$ include (i) an intermolecular fluxional process wherebythe dimer equilibrates with a small amount of a

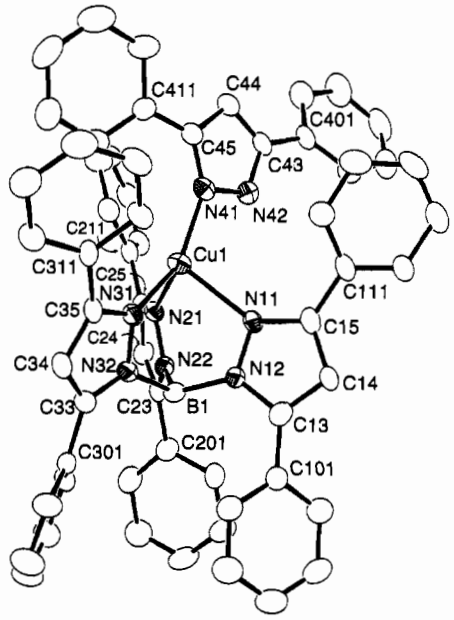

Figure 4. ORTEP drawing of $Tp^{Ph2}Cu(3,5\text{-}Ph_2pz) \cdot CH_2Cl_2$ showing 60% probability thermal ellipsoids for all non-hydrogen atoms (excluding the CH_2Cl_2 solvate molecule; labels provided for all atoms except the non-*ipso* carbons on the phenyl rings).

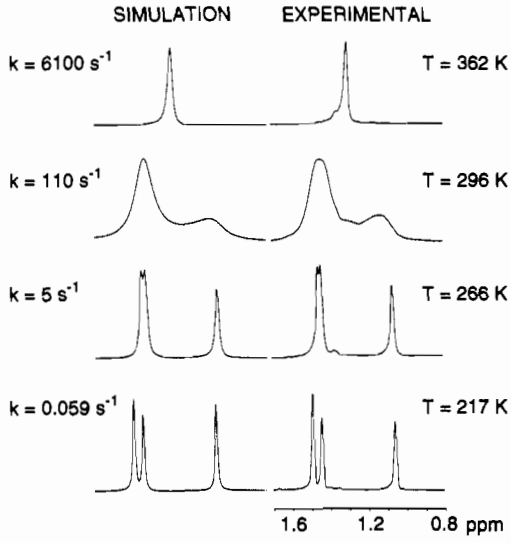

Figure 5. Selected variable-temperature ^1H NMR spectra and simulations of the *tert*-butyl region of $[Tp^{t\text{-}Bu}Cu]_2$ in toluene-d_8.

monomeric species with concomitant exchange of pyrazole environments or (ii) an intramolecular "pinwheel" motion of the $Tp^{t\text{-}Bu}$ ligands on the dicopper(I) core (Scheme II). The latter process bears some resemblance to the "tumbling" often observed in mononuclear η^3-Tp complexes (dissociative interchange of a pyrazolyl ring followed by chelate inversion and reassociation).[3]

Successful simulation of the experimentally determined ^1H NMR line shapes of the *t*-Bu resonances (Figure 5) was achieved by using a three-site exchange model implicit in the "pinwheel" mechanism (Scheme II). Although we could not observe another species in solution by ^1H NMR spectroscopy, we were not able to rule out the presence of a trace amount of a monomeric compound that might be an intermediate in the fluxional process. By plotting the rate constants calculated from line shape analysis of the NMR spectra according to the Eyring equation (Figure 6), activation parameters for the fluxional process were determined: $\Delta H^\ddagger = 11.7(5)$ kcal mol^{-1}, $\Delta S^\ddagger = -9(2)$ eu, and $\Delta G^\ddagger(295\ K) = 14.4(6)$ kcal mol^{-1}. The negative entropy of activation is consistent with the proposed intramolecular exchange mechanism and a constrained transition state (possibly involving coordination

Scheme II

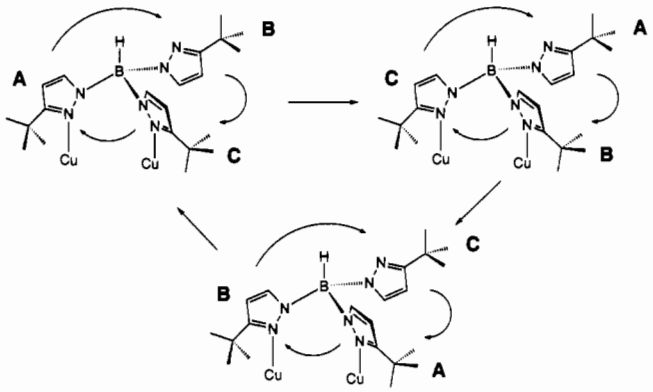

Note: Only one of the two $Tp^{t\text{-}Bu}$ ligands on $[Tp^{t\text{-}Bu}Cu]_2$ is shown for clarity. Also, process shown denotes overall interchange of rings, but does not indicate mechanism(s) of the exchange process.

of the free pyrazolyl ring to give an intermediate structure similar to—but energetically less favorable than—that of the ground-state structure of $[Tp^{Ph2}Cu]_2$; see Discussion).

In contrast, $[Tp^{Ph2}Cu]_2$ exhibits a single pyrazolyl hydrogen resonance in its ^1H NMR spectrum that remains sharp at temperatures as low as 213 K. As for its analog $[Tp^{Me2}Cu]_2$,[22] interconversion of pyrazolyl ring environments in solution is therefore too rapid to allow extraction of mechanistic information. Also as for $[Tp^{Me2}Cu]_2$, osmometric molecular weight measurements in toluene gave values significantly smaller than that calculated for the dimer, consistent with cleavage to ill-defined monomeric species. However, while we found that the ^1H NMR spectrum of $[Tp^{Me2}Cu]_2$ remained invariant over several days, the pyrazolyl peak in the spectrum of $[Tp^{Ph2}Cu]_2$ decreased in intensity and several new pyrazolyl resonances (unassigned as of yet) appeared over the course of several hours (initial rate of decrease in intensity of the pyrazolyl peak $\sim 3.0 \times 10^{-2}$ h^{-1}). In addition, in separate studies[25] we observed that freshly prepared solutions of $[Tp^{Ph2}Cu]_2$ only slowly reacted with NO, but if they were allowed to stand for several hours prior to exposure to the gas, there was an immediate reaction to form an orange NO adduct. Preliminary kinetics measurements showed that the rate of adduct formation in the presence of NO was similar to the initial rate of disappearance of the pyrazolyl peak in the ^1H NMR spectrum of $[Tp^{Ph2}Cu]_2$ in its absence. In contrast, rapid reaction of $[Tp^{Me2}Cu]_2$ with NO occurred irrespective of the amount of time the dimer was allowed to stand prior to gas exposure.[60] These data suggest that (i) the rate of cleavage of $[Tp^{Ph2}Cu]_2$ limits the rate of its reaction with NO, (ii) the rate of pyrazolyl interchange in $[Tp^{Ph2}Cu]_2$ is faster than its decomposition to lower molecular weight species, and (iii) the rate of decomposition of $[Tp^{Ph2}Cu]_2$ is slower than that of $[Tp^{Me2}Cu]_2$, unless cleavage of the latter is not rate limiting in NO adduct formation (i.e., NO reacts directly with the dimer).

Finally, the $Tp^{RR'}CuL$ compounds exhibited ^1H NMR spectra that were consistent with monomeric 4-coordinate structures for the complexes in solution. The spectra of all of these compounds contain a single set of peaks due to the hydrogens from three symmetry-equivalent pyrazolyl rings and corresponding resonances arising from the respective CH_3CN or 3,5-diphenylpyrazole coligands. However, the presence of a single sharp 4-pyrazolyl signal in the ^1H NMR spectrum of $Tp^{Ph2}Cu(3,5\text{-}Ph_2pz)$ is inconsistent on the basis of simple symmetry arguments with binding of the 3,5-diphenylpyrazole to the copper(I) ion in a static structure like that found by X-ray crystallography. The pyrazolyl rings in $Tp^{Ph2}Cu(3,5\text{-}Ph_2pz)$ are in different chemical

(60) Carrier, S. M.; Ruggiero, C. E.; Tolman, W. B. Unpublished results.

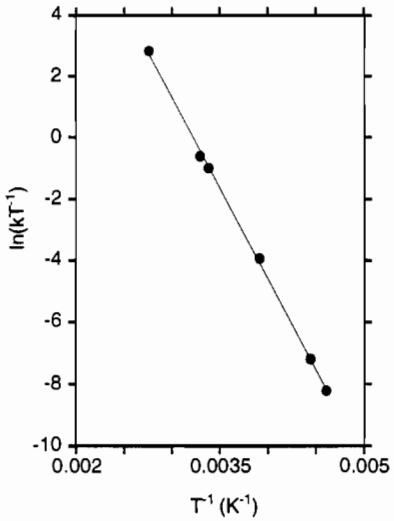

Figure 6. Eyring plot of the data calculated for the intramolecular fluxional process of $[Tp^{t\text{-}Bu}Cu]_2$ by line shape analysis of variable-temperature ^1H NMR spectra (see Figure 5).

environments in the solid state as a result of the binding of a sterically hindered C_{2v}-symmetric pyrazole to a C_{3v}-symmetric metal fragment. The observed equivalence of the Tp^{Ph2} pyrazolyl rings in the NMR spectrum can be explained by invoking a fluxional process that involves rapid dissociation, rotation, and reassociation of the 3,5-diphenylpyrazole ligand. Consistent with this hypothesis, the ^1H NMR spectrum of a sample of $Tp^{Ph2}Cu(3,5\text{-}Ph_2pz)$ to which 3,5-dimethylpyrazole had been added contained significantly broadened methyl and pyrazole hydrogen peaks, suggesting facile interchange of the 3,5-diphenyl- and 3,5-dimethylpyrazole ligands.

Electrochemistry. Cyclic voltammetry performed on freshly prepared solutions of the $[Tp^{RR'}Cu]_2$ and $Tp^{RR'}Cu(CH_3CN)$ complexes in CH_2Cl_2 with TBAH or (TBA)OTf electrolyte (0.1 M) revealed irreversible oxidations at rather high potentials (Table VI). The electrochemical behavior of the dimers $[Tp^{t\text{-}Bu}Cu]_2$ and $[Tp^{Ph2}Cu]_2$ may be readily explained by (i) the low coordination numbers for the complexes that favor the copper(I) state and (ii) the extensive structural rearrangements of the compounds that would be needed to attain geometries and coordination numbers amenable to copper(II) ions. The lack of chemical reversibility in the redox reactions of the monomeric $Tp^{t\text{-}Bu}Cu(CH_3CN)$ was more surprising, since $Tp^{t\text{-}Bu}Cu^{II}X$ (X = monodentate ligand) complexes are known to be relatively stable and isolable species.[5,23,61] Reasoning that dissociation of CH_3CN from $Tp^{t\text{-}Bu}Cu(CH_3CN)$ and a subsequent (undefined) structural rearrangement that occurred upon oxidation were ultimately responsible for its irreversible redox behavior, we added excess CH_3CN ($\sim$10% v/v) to the CH_2Cl_2 solution and CV's were recorded using TBAH and (TBA)OTf as electrolytes. With (TBA)OTf, an essentially chemically reversible redox process was observed which we ascribe to the $Tp^{t\text{-}Bu}Cu^{I}(CH_3CN)/Tp^{t\text{-}Bu}Cu^{II}(CH_3CN)^+$ couple (Figure 7a and Table VI). Consistent with this postulate, an identical CV was obtained from independently synthesized $Tp^{t\text{-}Bu}Cu^{II}(OTf)$.[23] This purple complex afforded a brown solution in CH_3CN/CH_2Cl_2 ($\sim$10%), presumably due to the formation of $[Tp^{t\text{-}Bu}Cu^{II}(CH_3CN)]OTf$. A similar CV was also obtained by addition of CH_3CN to a solution of $[Tp^{t\text{-}Bu}Cu]_2$ in CH_2Cl_2 with (TBA)OTf, suggesting that $Tp^{t\text{-}Bu}Cu(CH_3CN)$ can be formed by cleavage of $[Tp^{t\text{-}Bu}Cu]_2$ by the added ligand. However, an i_a/i_c value of 1.4 and a slightly different $E_{1/2}$ value in this instance indicated the presence of additional complicating reaction pathways. Interestingly, when TBAH was used as the supporting electrolyte in experiments

(61) Han, R.; Looney, A.; McNeill, K.; Parkin, G.; Rheingold, A. L.; Haggerty, B. S. *J. Inorg. Biochem.* **1993**, *49*, 105–121.

Table VI. Results from Cyclic Voltammetry Experiments on Solutions of Cu(I) Complexes

complex	electrolyte[a]	solvent[b]	E_{pa} (mV)[c]	$E_{1/2}$ (Mv)[d]	ΔE (mV)[e]	i_a/i_c[f]
$[Tp^{t\text{-}Bu}Cu]_2$	TBAH	CH_2Cl_2	1060			
	TBAOTf	CH_2Cl_2	1069			
		CH_3CN/CH_2Cl_2	926	852	149	1.4
$[Tb^{Ph2}Cu]_2$	TBAH	CH_2Cl_2	957			
		CH_3CN/CH_2Cl_2	904			
	TBAOTf	CH_2Cl_2	984			
		CH_3CN/CH_2Cl_2	927			
$Tp^{t\text{-}Bu}Cu(CH_3CN)$	TBAH	CH_2Cl_2	1005			
		CH_3CN/CH_2Cl_2	967			
	TBAOTf	CH_3CN/CH_2Cl_2	1016	930	171	1.1
$Tp^{Ph2}Cu(CH_3CN)$	TBAH	CH_2Cl_2	819			
		CH_3CN/CH_2Cl_2	710			
	TBAOTf	CH_2Cl_2	827			
		CH_3CN/CH_2Cl_2	724			
$Tp^{Ph2}Cu(3,5\text{-}Ph_2pz)$	TBAH	CH_2Cl_2	692	625	134	1.1
	TBAOTf	CH_2Cl_2	681	588	184	1.4

[a] All electrolyte solutions 0.1 M in TBAH or (TBA)OTf and ~5 mM in complex. [b] 10(2)% CH_3CN/CH_2Cl_2 v/v. [c] Scan rate v = 100 mVs^{-1}. Potentials are reported vs SCE (see Experimental Section). [d] $E_{1/2} = (E_{pa} + E_{pc})/2$. [e] $\Delta E = E_{pa} - E_{pc}$. [f] $i_{pa}/i_{pc} = [(i_{pc})_0/i_{pa} + 0.485(i\lambda)_0/i_{pa} + 0.086]^{-1}$, where i_{pa} is the peak current for the forward process, $(i\lambda)_0$ is the absolute current at the switching potential, and $(i_{pc})_0$ is the uncorrected return peak current measured from the current axis (see: Mabbott, G. A. *J. Chem. Educ.* **1983**, *60*, 697–702).

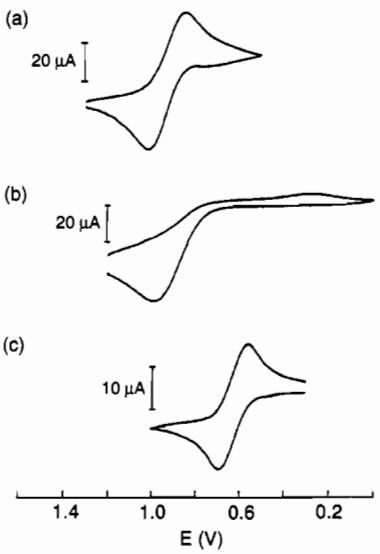

Figure 7. Cyclic voltammograms (scan rate = 100 mV s^{-1}; potentials vs SCE) of (a) 0.01 M solution of $Tp^{t\text{-}Bu}Cu(CH_3CN)$ in 10(2)% CH_3CN/CH_2Cl_2 (v/v) with 0.1 M (TBA)OTf, (b) same solution as in (a) except with 0.1 M TBAH electrolyte, and (c) 0.006 M solution of $Tp^{Ph2}Cu(3,5\text{-}Ph_2pz)$ in CH_2Cl_2 with 0.1 M TBAH.

involving $Tp^{t\text{-}Bu}Cu(CH_3CN)$, even in the presence of CH_3CN, only an irreversible oxidation wave and a reduction wave at considerably lower potential and current were observed (Figure 7b). Since the only difference between the conditions used for the CV experiments shown in Figure 7a,b was the nature of the electrolyte, we surmise that reaction of PF_6^- with the species formed upon oxidation of $Tp^{t\text{-}Bu}Cu(CH_3CN)$ was responsible for the irreversibility evident in the latter CV. Fluoride extraction from PF_6^- is one possibility for which there is literature precedent, the reported isolation of copper(II)–fluoride complexes upon oxidation of Cu(I) complexes by dioxygen in the presence of PF_6^- being particularly noteworthy.[62] Especially tight binding of PF_6^- to the Cu(II) species also might be responsible for the irreversible behavior observed.[63-65]

For the case of $Tp^{Ph2}Cu(CH_3CN)$, CV's indicative of chemically reversible redox reactions could not be obtained by addition of excess CH_3CN or by variation of the electrolyte. The smaller size of the ligand substituents in $Tp^{Ph2}Cu(CH_3CN)$ compared to those in $Tp^{t\text{-}Bu}Cu(CH_3CN)$ may allow either more drastic copper geometry reorganization or binding of a fifth exogenous ligand (CH_3CN?) upon oxidation, both of which would contribute to irreversibility in the CV experiments. Indeed, we[60] and others[5] have obtained independent evidence supporting solvent coordination to 4-coordinate divalent metal complexes that contain the Tp^{Ph2} or Tp^{Ph} ligand.

These possible sources of irreversibility are apparently overcome in $Tp^{Ph2}Cu(3,5\text{-}Ph_2pz)$, the only complex to exhibit chemically reversible electrochemistry in the absence of added CH_3CN (Figure 7c and Table VI). Interconversion of $Tp^{Ph2}Cu^{I}(3,5\text{-}Ph_2pz)$ and $Tp^{Ph2}Cu^{II}(3,5\text{-}Ph_2pz)^+$ appears likely, the stronger binding of 3,5-diphenylpyrazole to Cu(II) and its greater steric bulk compared to CH_3CN being key factors which inhibit the type of deleterious side reactions that complicate the electrochemistry of $Tp^{Ph2}Cu(CH_3CN)$. Attempts to confirm this hypothesis by isolating $Tp^{Ph2}Cu(3,5\text{-}Ph_2pz)^+$ are underway.

Discussion

The observed solution- and solid-state properties of the compounds prepared in this study exemplify important aspects of Cu(I) coordination chemistry in a set of complexes with homologous ligands. First, the ability of Cu(I) ions to adopt 2-, 3-, or 4-coordinate structures according to the steric influences dictated by attached ligands is nicely demonstrated by these compounds. In particular, the dimers $[Tp^{t\text{-}Bu}Cu]_2$ and $[Tp^{Ph2}Cu]_2$, along with the analogs $[TpCu]_2$ and $[Tp^{Me2}Cu]_2$ reported previously,[22] provide a unique set of structurally characterized and homoleptic molecules with ligands that only differ significantly with respect to their steric properties. Copper(I) coordination number tracks with the size of the 3-pyrazolyl substituents within this set, from 2 when R = *t*-Bu, 3 when R = Ph, 3 plus a weak additional interaction with the "semibridging" pyrazolyl group when R = Me, to 4 when R = H (Figure 8). For the case of Tp^{iPr2}, a complex formulated as $[Tp^{iPr2}Cu]_n$ was isolated by Kitajima and co-workers which was proposed to adopt a monomeric 3-coordinate structure on the basis of its high reactivity with dioxygen.[19] On the basis of our results, and considering that the size of an isopropyl group lies close to that of a *tert*-butyl substituent, we suggest that it exists primarily as a dimer with 2-coordinate Cu(I) ions analogous to $[Tp^{t\text{-}Bu}Cu]_2$. The high reactivity with dioxygen observed for the Tp^{iPr2} complex is inconsistent with such a geometry in solution, however, as linear 2-coordinate Cu(I) species are known to be inert toward O_2.[66,67]

(62) Jacobson, R. R.; Tyeklár, Z.; Karlin, K. D.; Zubieta, J. *Inorg. Chem.* **1991**, *30*, 2035–2040.
(63) Beck, W.; Sünkel, K. *Chem. Rev.* **1988**, *88*, 1405.
(64) Hill, M. G.; Lamanna, W. M.; Mann, K. R. *Inorg. Chem.* **1991**, *30*, 4687–4690.
(65) Honeychuck, R. V.; Hersh, W. H. *Inorg. Chem.* **1989**, *28*, 2869–2886.
(66) Sorrell, T. N.; Jameson, D. L. *J. Am. Chem. Soc.* **1983**, *105*, 6013–6018.

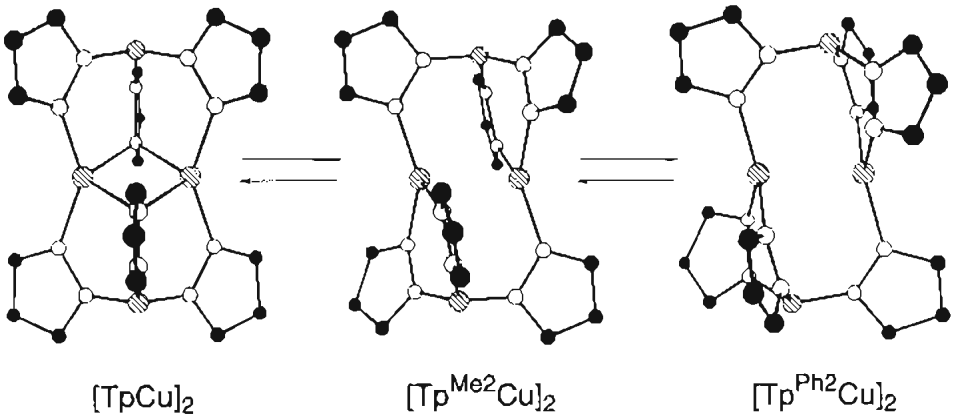

Figure 8. Drawings prepared from the X-ray crystal structure coordinates of $[Tp^{RR'}Cu]_2$ (R = R' = H,[22] Me,[22] or Ph) viewed perpendicular to the Cu···Cu vectors (pyrazolyl substituents not shown).

This apparent discrepancy can be resolved by postulating formation of a small amount of an unobserved, yet highly reactive, monomer derived from $[Tp^{iPr2}Cu]_2$ in solution. The existence of such a species for dissolved $[Tp^{t\text{-}Bu}Cu]_2$ is not ruled out by the data we have collected (*vide infra*) and might help to explain our observation of more facile reaction of $[Tp^{t\text{-}Bu}Cu]_2$ with nitric oxide compared to the reaction of $[Tp^{Ph2}Cu]_2$.[24,25]

A second and related feature of Cu(I) coordination chemistry that is demonstrated by the complexes reported herein is the smooth variation in Cu–N bond length with coordination number. The average $Cu–N_{pz}$ distances for $[Tp^{t\text{-}Bu}Cu]_2$, $[Tp^{Ph2}Cu]_2$, and $Tp^{Ph2}Cu(3,5\text{-}Ph_2pz)$ are 1.88, 1.99, and 2.09 Å, respectively. These values are quite similar to the average bond lengths for Cu(I) complexes of N-donor ligands noted previously: 1.88 Å for 2-coordination, 1.97 Å for 3-coordination, and 2.04 Å for 4-coordination.[45,68] Clearly, decreased intramolecular nonbonding interactions in the complexes of low coordination number are responsible for the shorter metal–ligand bond distances in complexes of the spherically symmetric (d^{10}) Cu(I) ion.

Third, the lability in solution typical for Cu(I) complexes is manifested by the intra- and/or intermolecular fluxionality observed for the compounds we have prepared. Similar to what was noted previously for the dimers $[TpCu]_2$ and $[Tp^{Me2}Cu]_2$,[22] deceptively simple ^1H NMR spectra were observed for $[Tp^{Ph2}Cu]_2$ and $Tp^{Ph2}Cu(3,5\text{-}Ph_2pz)$, which suggested that facile ligand exchange processes occur in solution that render the respective pyrazolyl groups chemically equivalent. None of these processes could be slowed sufficiently by lowering the temperature to allow mechanistic analysis via line shape modeling. More indirect data such as those obtained from molecular weight measurements and reactivity studies for $[Tp^{Ph2}Cu]_2$ and NMR spectra of solutions containing an exogenous pyrazole for $Tp^{Ph2}Cu(3,5\text{-}Ph_2pz)$ suggest that dimer cleavage or ligand dissociation/reassociation occurs in the respective cases. In $[Tp^{t\text{-}Bu}Cu]_2$, however, the greater steric hindrance provided by the *tert*-butyl groups slows the fluxionality sufficiently to allow mechanistic analysis, and on the basis of successful line shape modeling, we postulate averaging of the *tert*-butylpyrazolyl rings via (i) a process involving a trace amount of an unobserved monomeric intermediate or (ii) an intramolecular rotation of the $Tp^{t\text{-}Bu}$ ligand about the dicopper(I) core (Scheme II).

It is interesting to view this latter intramolecular motion of the $Tp^{t\text{-}Bu}$ ligand in the context of the array of solid-state structures now available for the set of dimeric $[Tp^{RR'}Cu]_2$ complexes. For instance, one pathway for $Tp^{t\text{-}Bu}$ movement and pyrazolyl ring equilibration might involve a shift of a terminally bound pyrazolyl group to a bridging position, with continuation along this route resulting in this pyrazolyl unit adopting a terminal coordination mode on the second metal ion. The structures of $[Tp^{Ph2}Cu]_2$, $[Tp^{Me2}Cu]_2$, and $[TpCu]_2$ represent possible "snapshots" along this reaction pathway,[69] the respective terminal, "semibridging", and bridging modes of a pyrazolyl ring in these compounds representing intermediate structures that may lie along the potential energy surface for the fluxional process (Figure 8). Alternatively, the structure of $[Tp^{t\text{-}Bu}Cu]_2$ might be viewed as an intermediate in a different mechanism involving dissociation of a pyrazolyl ring from one metal center and reassociation at the second.

Turning to the electrochemical data (Table VI), the most striking results are the large positive oxidation potentials >0.6 V for all of the monomeric complexes and the more informative large positive $E_{1/2}$ values for the $Tp^{t\text{-}Bu}Cu^{I}(CH_3CN)/Tp^{t\text{-}Bu}Cu^{II}(CH_3CN)^+$ and $Tp^{Ph2}Cu^{I}(3,5\text{-}Ph_2pz)/Tp^{Ph2}Cu^{II}(3,5\text{-}Ph_2pz)^+$ couples. Redox potentials for copper complexes with N_4 donor sets are generally much lower,[70–72] although detailed comparisons are hindered by the use of different solvents and experimental conditions among different researchers. Of the myriad of factors which can perturb Cu(I)/Cu(II) redox potentials, stabilization of the Cu(I) state and destabilization of the Cu(II) state via enforcement of a pseudotetrahedral geometry by the sterically hindered $Tp^{RR'}$ ligands would appear to be the best explanation for the data we have collected. The use of sterically hindered or otherwise geometrically constrained ligands to induce deviations from tetragonal geometries and raise $E_{1/2}$ values for copper complexes containing N_4 donor ligand environments has been reported,[70–73] but in most cases the potentials are not as high as those we have observed. Geometric constraints were found to induce redox potentials similar to those of the hindered $Tp^{RR'}$ ligands in a series of trigonal pyramidal Cu(I) complexes of tris(pyrazolylethyl)amines; for the Cu(I) complex of tris(3,5-di-*tert*-butylpyrazolyl)ethyl)amine, $E_{1/2}$ = +0.94 V vs SCE in CH_3CN.[74] For the compounds we have studied, the highest $E_{1/2}$ (+0.93 mV vs SCE in CH_2Cl_2) was recorded for $Tp^{t\text{-}Bu}Cu(CH_3CN)$, which contains the most hindered $Tp^{t\text{-}Bu}$ ligand. The oxidation potentials for the complexes containing the Tp^{Ph2} ligand are generally lower than that of $Tp^{t\text{-}Bu}Cu(CH_3CN)$, despite the fact that IR analyses of $Tp^{RR'}CuL$ (L = CO and NO) have shown that the Tp^{Ph2} ligand is more electron withdrawing than $Tp^{t\text{-}Bu}$ [e.g., ν(CO) = 2069 cm^{-1} for $Tp^{t\text{-}Bu}Cu(CO)$[24,25] and 2086 cm^{-1} for $Tp^{Ph2}Cu(CO)$[19]]. We hypothesize that the greater "tetrahedral enforcing" ability

(67) Sanyal, I.; Strange, R. W.; Blackburn, N. J.; Karlin, K. D. *J. Am. Chem. Soc.* **1991**, *113*, 4692–4693.
(68) Hathaway, B. J. In *Comprehensive Coordination Chemistry*; Wilkinson, G., Gillard, R. D., McCleverty, J. A., Eds.; Pergamon Press: Oxford, U.K., 1987; Vol. 5; pp 533–774.
(69) Bürgi, H. B.; Dunitz, J. *Acc. Chem. Res.* **1983**, *16*, 153–161.
(70) Patterson, G. S.; Holm, R. H. *Bioinorg. Chem.* **1975**, *4*, 257–275.
(71) Karlin, K. D.; Gultneh, Y. *Prog. Inorg. Chem.* **1987**, *35*, 219–328.
(72) Zanello, P. *Comments Inorg. Chem.* **1988**, *8*, 45–78.
(73) Knapp, S.; Keenan, T. P.; Zhang, X.; Fikar, R.; Potenza, J.; Schugar, H. J. *J. Am. Chem. Soc.* **1990**, *112*, 3452–3464 and references therein.
(74) Sorrell, T. N.; Jameson, D. L. *Inorg. Chem.* **1982**, *21*, 1014–1019.

of the latter outweighs the more subtle electronic influences of the ligand substituents. However, differences between the other ligands present [i.e., CH_3CN vs 3,5-diphenylpyrazole in $Tp^{t\text{-}Bu}Cu(CH_3CN)$ and $Tp^{Ph2}Cu(3,5\text{-}Ph_2pz)$, respectively] also influence the magnitude of the redox potentials, necessitating future investigations of more similar complexes of the $Tp^{t\text{-}Bu}$ and Tp^{Ph2} chelates in order to more definitively assess substituent effects on their electrochemistry. Such studies are particularly important in light of the apparent relationship of the redox potentials of $Tp^{t\text{-}Bu}Cu(CH_3CN)$ and $Tp^{Ph2}Cu(3,5\text{-}Ph_2pz)$ to the electronic structures of biologically relevant NO adducts we have prepared in separate studies.[24]

Concluding Remarks

The wealth of solid-state and solution structural data now available for $Tp^{RR'}Cu(I)$ complexes allows us to draw several conclusions regarding the relationship of such information to their observed reactivity with O_2 and NO. For the $Tp^{t\text{-}Bu}$ and probably the Tp^{iPr2} ligands having the largest 3-substituents, dimers with 2-coordinate Cu(I) ions predominate in the solid state and in solution. Despite the previously demonstrated lack of reactivity of 2-coordinate Cu(I) complexes of N-donor ligands with O_2,[66,67] the complexes react rapidly with O_2 and NO to afford readily isolable dinuclear μ-(η^2:η^2)-peroxo[19] or mononuclear η^1-nitrosyl[24,25] adducts, respectively. Apparently, the sterically bulky substituents play multiple roles: (i) forcing the Cu(I) ions to adopt 2-coordinate geometries, (ii) stabilizing higher coordinate reaction products by forming a protective pocket about the bound diatomic species, and (iii) possibly inducing the formation of trace amounts of highly reactive monomeric species in solution that rapidly bind the paramagnetic gases. The Tp^{Ph2} and Tp^{Me2} ligands form Cu(I) dimers having similar solid-state structures, but with higher metal coordination numbers and differing solution behavior consistent with the differing size of their pyrazolyl substituents. The low reactivities of freshly prepared solutions of $[Tp^{Ph2}Cu]_2$ with NO and the much higher reactivity of $Tp^{Ph2}CuL$ (L = CH_3CN or 3,5-Ph_2pz) with NO, older solutions of $[Tp^{Ph2}Cu]_2$ with NO,[25] and $Tp^{Ph2}Cu(Me_2CO)$ with O_2[19] suggest that the dimer $[Tp^{Ph2}Cu]_2$ with 3-coordinate Cu(I) ions is much less reactive than those dimers that have 2-coordinate metals, probably because the monomeric species either prepared independently or derived from dimer cleavage that bind the gases rapidly are formed less readily. The behavior of $[Tp^{Me2}Cu]_2$ is anomalous because although it appears to cleave rapidly in solution and to immediately react with NO, its reaction with O_2 is sluggish.[75] Also, different final products are formed in its reactions with O_2 (oxidation to $Tp^{Me2}{}_2Cu$)[75] and NO [disproportionation to N_2O and $Tp^{Me2}Cu(NO_2)$][60] compared to the reactions of more hindered complexes, further complicating structure/reactivity correlations among the $Tp^{RR'}Cu^{I}$ compounds.

Acknowledgment. We thank Professor Doyle Britton for his work on the X-ray crystal structure determinations, Professor Thomas Sorrell for providing a preprint, and the reviewers for helpful comments. Financial support for this research was provided by the National Institutes of Health (Grant GM47365), the Searle Scholars Program/Chicago Community Trust, the Exxon Education Foundation, and the University of Minnesota.

Supplementary Material Available: A fully labeled ORTEP drawing of $[Tp^{Ph2}Cu]_2$ and complete lists of bond lengths and angles, atomic positional parameters, and final thermal parameters for nonhydrogen atoms for $[Tp^{t\text{-}Bu}Cu]_2$, $[Tp^{Ph2}Cu]_2$, and $Tp^{Ph2}Cu(3,5\text{-}Ph_2pz)$ (Tables S1–S4, S5–S8, and S9–S12, respectively) (27 pages). Ordering information is given on any current masthead page.

(75) Kitajima, N.; Moro-oka, Y.; Uchida, A.; Sasada, Y.; Ohashi, Y. *Acta Crystallogr.* **1988**, *C44*, 1876–1878.